Nuclear Effects in Quasi-Elastic and Delta Resonance Production at Low Momentum Transfer

A THESIS
SUBMITTED TO THE FACULTY OF THE GRADUATE SCHOOL
OF THE UNVERSITY OF MINNESOTA
BY

John Gibney Demgen

IN PARTIAL FULFILMENT OF THE REQUIREMENTS
FOR THE DEGREE OF
MASTER OF SCIENCE

Advisor: Dr. Richard Gran

August 2015

Acknowledgments

Thanks to MINERvA for immediately being so accepting and to all of those who were helpful and friendly at the lab.

Thanks to Mithila, Mudit, Dan, Jake, Jordan, Matt, and everybody else in the program at Duluth for keeping me level for two years, even when classes were stressful.

Thanks to Ethan for a quality year spent doing research together, and Phil for joining the analysis team. Also, Alec and Jake for jumping in and helping this summer.

Thanks to my thesis committee, and the other faculty in the physics department at Duluth. Your wealth of knowledge was very helpful over the past two years.

Rik, you are an excellent advisor and I'm glad you sold me to on your “pet project.” Thanks for helping navigate school and career decisions the past year.

Thanks to Mom, Dad, the family and the extended “family” at home for being supportive always, including when I moved to Duluth at the drop of a dime.

Abstract

Analysis of data collected by the MINERvA experiment is done by showing the distribution of charged hadron energy for interactions that have low momentum transfer. This distribution reveals major discrepancies between the detector data and the standard MINERvA interaction model with only a simple global Fermi gas model. Adding additional model elements, the random phase approximation (RPA), meson exchange current (MEC), and a reduction of resonance delta production improve this discrepancy. Special attention is paid to resonance delta production systematic uncertainties, which do not make up these discrepancies even when added with resolution and biasing systematic uncertainties. Eye-scanning of events in this region also show a discrepancy, but we were insensitive to two-proton events, the predicted signature of the MEC process.

Contents

List of Tables

List of Figures

1. Motivation

Neutrino scattering experiments depend on Monte Carlo (MC) simulations to compare their detector data to how well they understand the processes involved. Neutrino scattering interactions are simulated for the different types of neutrino scattering and simulated in the detector environment. How well the processed detector data matches the set of simulated events ideally matches up flawlessly, signaling that physicists have very accurately modeled the mechanics of neutrino scattering. Figures 1[1] and 2 show the distribution of events for the MINERvA experiment, compared to its MC simulation. The figures differ by the energy values used in the x axis but their story is the same.

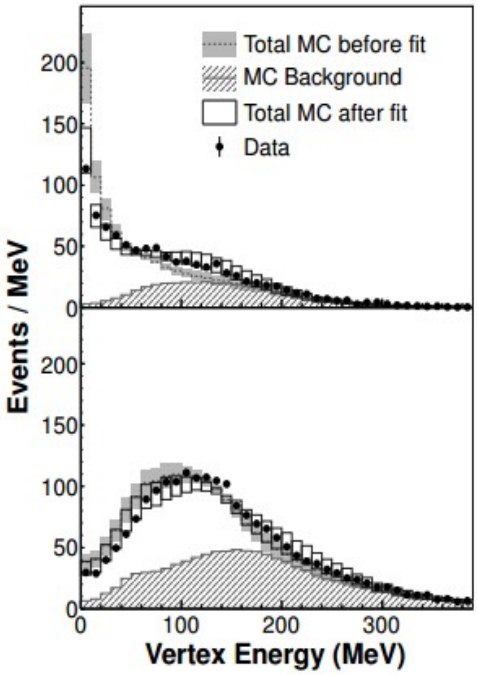

Figure 1: Results from the MINERvA PRL publication for quasi-elastic events. Top plot Q^2 < 0.2 GeV, bottom Q^2>0.2 GeV [1]

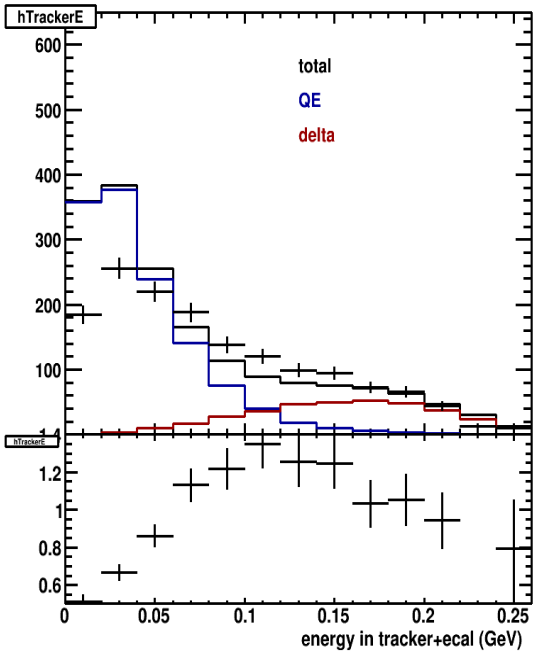

Figure 2: Low q_3 distribution (q_3 < 0.4 GeV) for the MINERvA detector. Data points are in black, simulated events are solid black lines. Subsets of the simulated events are described by the blue and red lines

The MC simulation for the MINERvA experiment contains an incomplete default interaction model. Figure 1 was published by the MINERvA collaboration as their primary result of their study on quasi-elastic neutrino-nucleon scattering within a carbon target. The x-axis value, vertex energy, is the passive-corrected energy observed in a region surrounding the point of interaction “vertex” of the muon-neutrino carbon scattering event.

Figure 2 is a preview of the analysis in this thesis. It is the distribution of the measured hadronic energy with three-momentum transfer less than 0.4 GeV. The x-axis shows energy in the tracker and electromagnetic calorimeter regions of the MINERvA detector. This hadronic energy is similar to the one presented in the 2013 MINERvA paper, but is not limited to region near the vertex. In both plots the MC simulation has over predicted the number of data events in the lowest energy bins, and has under predicted the data events near 100 MeV in Fig. 1, and starting at 0.06 GeV. The disagreement shown in both plots tells the same story, additional model effects are needed for the MINERvA MC simulation to accurately model the data taken by the detector.

1.1 Quasi-elastic Scattering

Quasi-elastic (QE) scattering is the most simple neutrino scattering event. This scattering process is the most like standard elastic billiard ball collisions. Figure 3 shows the mechanics of the QE process. For the muon neutrino case, an incoming neutrino exchanges a W^+ boson with a neutron. The W^+ particle is a charged force carrier for the weak nuclear force. The neutron in Fig. 3 is converted and scatters as a proton while the neutrino is converted to its leptonic partner, the negatively charged muon. For the anti-neutrino case this process would replace the W^+ with

its negatively charged partner the W^-, replace the neutron with a proton converting to neutron, and result in an outgoing anti-muon. The neutrino scattering reaction in Fig. 3 is

$$\nu_\mu + n \rightarrow \mu^- + p \qquad (1)$$

It is possible that the proton interacts with other nucleons as it exits the nucleus. This means that multiple nucleons can enter the detector as a result of the quasi-elastic scattering although it starts as only one proton. This type of scattering is called quasi-elastic because off energy transferred by the virtual W boson between the leptonic system and the hadronic system. Energy transfer constitutes as inelastic scattering, but in this case the energy transferred is much smaller than the energy of the incident neutrino.

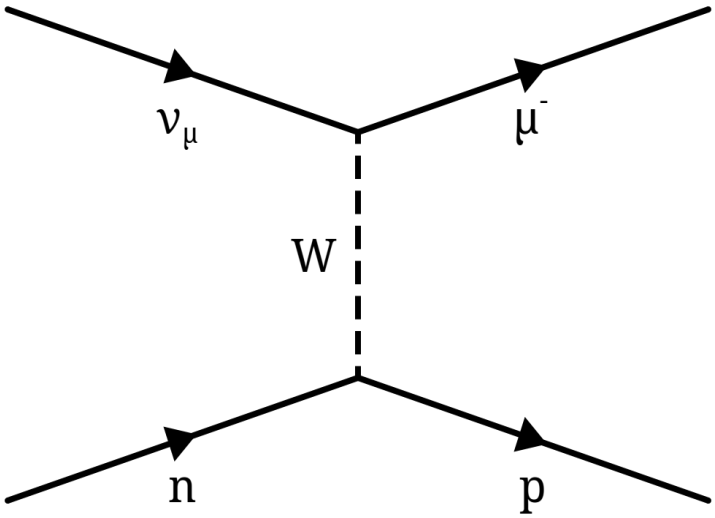

Figure 3: Feynman diagram for charged current quasi-elastic neutrino scattering.

1.2 Delta Resonance Production

Delta resonance production is more complicated than the QE process. The proton and neutron are bound states of three quarks. The proton is composed of an uud configuration while the neutron is udd. These represent the ground states of any three quark system. The uuu and ddd configurations are not allowed to have all three quarks in the ground state because of the Pauli exclusion principle; there can only be two up or two down quarks in the lowest energy state, one spin up and one spin down. The delta particles are the first excited states of three quark systems comprised of up and down quarks.

The delta baryon comes in four different types, corresponding to charges of +2 (uuu), +1 (uud), 0 (udd) and -1 (ddd). For neutrino scattering, there is production of Δ^{++} and Δ^{+} particles from resonance production. Figure 4 shows one mode of delta production, where a neutrino scatters off a neutron to produce a Δ^{+} particle. The reaction is

$$\nu_\mu + n \rightarrow \mu^- + \Delta^+ \qquad (2)$$

with the Δ^{+} particle decaying one or the other nucleon three-quark ground state

$$\Delta^+ \rightarrow \pi^+ + n \quad \text{or} \qquad (3)$$

$$\Delta^+ \rightarrow \pi^0 + p \qquad (4)$$

within the nucleus. This is due to the lifetime of the delta particles which is on the order of 10^{-24} seconds. If the neutrino instead reacts with a bound proton, the reaction becomes

$$\nu_\mu + p \rightarrow \mu^- + \Delta^{++} \quad (5)$$

with the Δ^{++} particle decaying in the nucleus to

$$\Delta^{++} \rightarrow \pi^+ + p \quad (6)$$

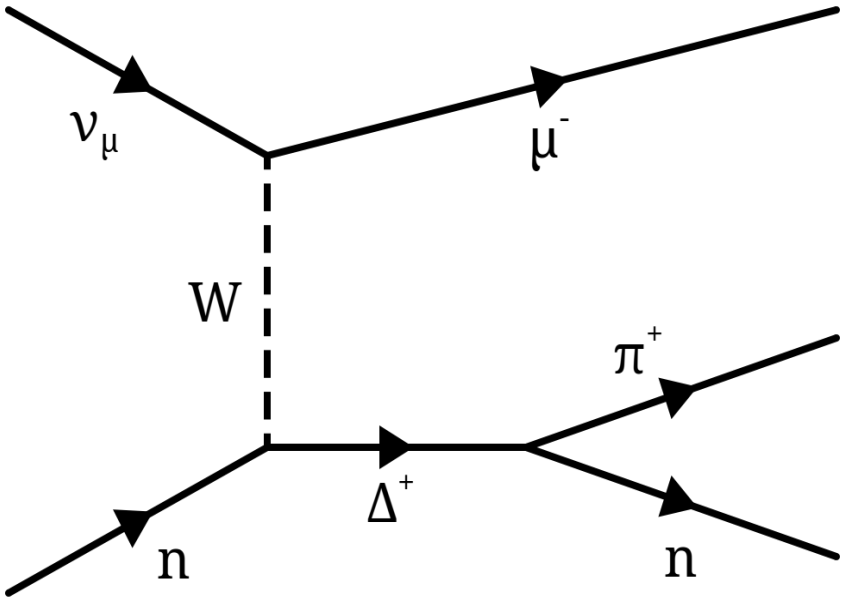

Figure 4: Delta resonance production in neutrino scattering. In this instance the delta decays into a charged pion and a neutron

The delta particle cannot be observed directly because it decays in the nucleus. The troubling feature of the delta is its short lifespan. The delta particle decays with a mean lifetime on the order of 10^{-24} seconds, which does not give the delta enough time to escape the nucleus. The result is that delta resonance production is identified by the delta decay products.

The decay products of the delta particle will have the same invariant mass as the delta particle. Invariant mass is the mass in the rest frame of a particle. If a particle decays, the invariant mass can be computed from the decay products. Measuring the latter is one way to confirm the production of a delta particle. The invariant mass squared, W^2 is defined as the sum of the squared energies minus the sum of the squared momentums of the i decay products

$$W^2 = (\Sigma_i E_i)^2 - (\Sigma_i P_i)^2 \qquad (7)$$

If this was a delta, W computed from the measured hadronic system would be near 1232 MeV/c^2. In contrast, the QE reaction discussed previously would have W equal to the proton mass at 938 MeV/c^2.

The difficulty in this invariant mass reconstruction lies in neutral particles; if the pion re-scatters neutrons and is absorbed into the nucleus, invariant mass reconstruction from the individual hadrons becomes difficult. Neutrons are uncharged and thus do not deposit much energy in the detector. If you can measure the kinematics of the lepton system, in our case the neutrino and the muon, then the invariant mass is

$$W^2 = M^2 - Q^2 + 2M(E_\mu - E_\nu) \qquad (8)$$

where the context of this equation and the variable Q^2 are introduced in the next sub-section.

Pion identification is the other way to identify a delta production event has occurred. For the neutrino mode equations 3 and 6 show π^+ production in delta decay and equation 4 shows π^0 production in delta decay. The mean lifetime of a

neutral pion, which are produced less often than the charged pions, is on the order of 10^{-17} seconds. Neutral pions will normally not make it out of the nucleus, but will deposit energy from a pair of gamma rays that will convert to energetic electromagnetic showers on average 30 cm distance from the event vertex. Charged pions, produced much more often by delta decay have a lifetime of 26 ns. At the speed of light they could travel 10 meters, but because they are charged, they lose energy ionizing atoms as they travel. In the end they travel some distance proportional to how much energy they have, and positive pions will decay frequently.

Some delta resonance events do not have a pion in the final state, among the particles exiting the nucleus into the detector. It is possible that the pion and nucleons scatter off other nucleons as they leave the nucleus. These are called final state interactions (FSI) or intra-nuclear re-scattering. In the default Genie model, 25% of delta events do not have a charged pion in the final state. Identification of the delta based on the appearance of a pion is much easier than that for an event in which the pion undergoes FSI and multiple nucleons exit the nucleus. Since neutral particles do not deposit energy in our detector, FSI can cause lost energy in the form of neutrons which do not decay in the event window. Since pions are so important to identifying delta production they can be categorized as delta production with a pion, and delta production without a pion.

1.3 Other Reactions

As energies increase, it is also possible to produce other three quark resonances. The delta is the first resonance at W = 1232 MeV/c^2 but as higher energies are transferred to the nucleon system other resonances can occur. These resonance

particles are similarly short lived, with mean lifetimes in the 10^{-23} seconds range.

Deep inelastic scattering (DIS) occurs when the W^+ boson acquires enough energy to probe the individual quarks inside the nucleon. Deep inelastic scattering occurs off of the up and down valence quarks in the nucleon as well as any quarks in the virtual sea of quarks which are constantly popping in and out of existence. The quark is "knocked" out of the nucleus, but because of quark confinement the result is a shower of hadrons. This analysis will not include higher resonance or DIS events.

1.4 Scattering Kinematics

For full analysis of the discrepancies between the detector data and MC simulation and the candidate model additions we must define important kinematics of the scattering process. These energy and invariant quantities include energy transfer, three-momentum transfer, and Q^2. Energy transfer, often denoted as q_0 or called the hadronic recoil energy, is defined in equation 1 as the energy transferred from the incoming neutrino to the hadronic system in the detector.

$$\text{Recoil } E = q_0 = E_\nu - E_\mu \tag{9}$$

where E_ν is the energy of the incoming neutrino and E_μ is the energy of the outgoing muon. This quantity is the energy of the virtual W^+ boson in figures 3 and 4. Three-momentum transfer is the momentum transferred from the neutrino to the hadronic system. Three-momentum is defined as

$$q_3 = p_\nu - p_\mu \tag{10}$$

which is the momentum of the W^+ boson in figures 3 and 4. We can use these two quantities, recoil energy and three-momentum transfer, to examine the default cross section for the Genie simulation model.

A cross section is a measurement of how frequently a type of neutrino scattering event will occur. The cross section has units such that if it is multiplied by the incident neutrinos per area per second and the number of target nuclei, the result is the number of scattering events per second. Figure 5 is the default Genie double differential cross section. Double differential refers to there being two kinematic variables needed to calculate the cross section. The higher intensities in Fig. 5 correspond to regions of q_0 and q_3 space where more scattering events will occur.

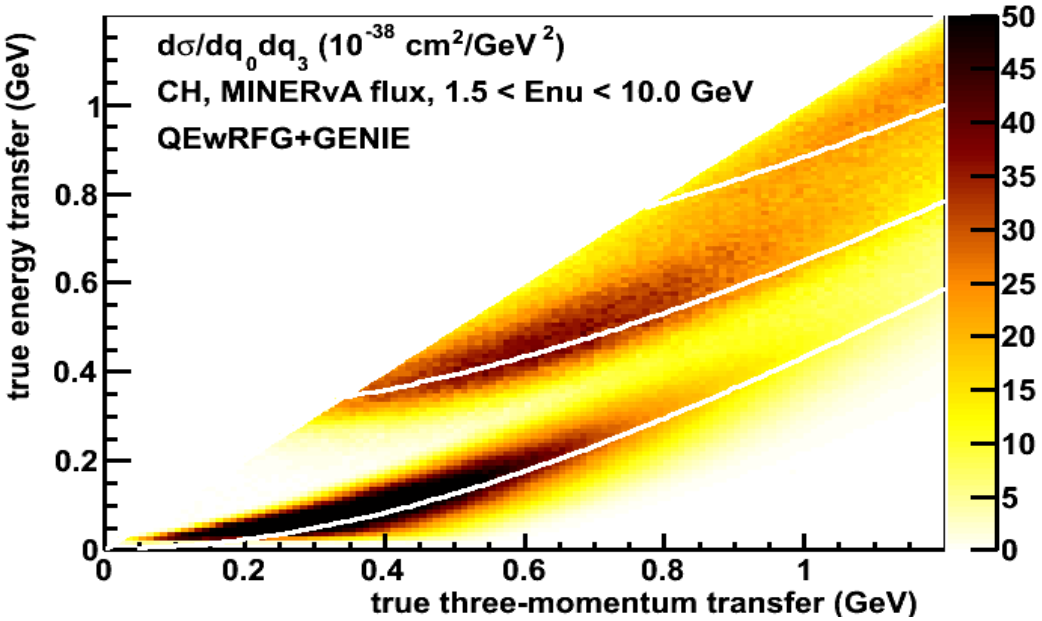

Figure 5: Intensity plot of the double-differential cross section on carbon for the standard Genie model. Lines of constant increasing invariant mass (W) are shown

If we define q as the four momentum transfer vector (q_0, q_3) then Q^2 is defined as the negative square of this four momentum vector

$$Q^2 = -q^2 = q_3^2 - q_0^2 \quad (11)$$

Q^2 is an invariant quantity, meaning it will have the same value in all reference frames including the lab frame and the frame of the outgoing muon.

Because we don't know the neutrino energy event by event, but can measure the energy of the muon and the hadronic system, we come at these quantities the other way around

$$E_\nu = E_\mu + q_0 \quad (12)$$

If the energy of the neutrino E_ν, the energy of the muon E_μ, the angle of the muon θ_μ, the recoil energy q_0, and the three momentum q_3 are known then Q^2 is defined as

$$Q^2 = 2E_\nu(E_\mu - q_3\cos\theta_\mu) - M_\mu^2 \quad (13)$$

where M_μ is the mass of the muon at 105.658 Me/c^2. The muon quantities are measured in the MINOS detector while the momentum and energy transfer are measured in the MINERvA detector.

The contours in figure 5 are constant invariant mass W values for various neutrino scattering events. The first contour from the bottom axis corresponds to the QE process, with W = 938 MeV, or the mass of the proton. The second contour is the delta resonance with W = 1232 MeV. When using only these processes, there is an

empty region (called the dip region) between the QE and the delta, which is an important feature of the nominal model. The required energy transfer to excite the proton into the delta state if both are at rest is the difference between the invariant masses, or q_0 = 294 MeV. This would be the difference between the first two contours if the second extended to the q_3 = 0 axis. The third contour is the next resonance at W = 1520 MeV.

The rate of these reactions is modified by the environment in the nucleus. Pauli blocking is the name given to reactions that do no happen because of the Pauli exclusion principle which states that two fermions (particles with half integer-spin,) cannot occupy the same quantum state. Any reaction in the Genie simulation that does not give enough energy to the nucleon to kick it into an unoccupied energy state are rejected.

Events in Figure 5 are smeared around the contours of constant W because of nuclear effects. Momentum of the target nucleon contributes to the smearing of events around the contours of constant W. Although the carbon nucleus is effectively at rest in the detector, the individual nucleons move about the nucleus. Traditionally the momentum of particles in the nucleus is modeled as a global Fermi gas. This is the red line in Fig. 6, showing that the momentum increases as function of the distance from the center of the nucleus.

The measured distribution of momentum for nucleons in the nucleus is show in Fig. 6 as the solid blue line. This has a long tail to high momentum, as opposed to the peaked distribution truncated at 250 MeV/c.

A Fermi gas is the standard way to model the spacial and momentum components of electrons or nucleons in an atom. The local Fermi Gas is a global Fermi gas that

depends on nuclear density. This produces a change in the global Fermi gas depending if the target nucleon was in the middle or edge of the nucleus. This model is more like the measured momentum, yet is simple enough to implement in simulation codes. The difference between these two approaches is noticeable for hypothetical scattering on a free proton or neutron, but is negligible for the analysis described here. Pauli blocking is also apparent in figure 6[2]; If the target nucleon does not achieve at least 250 MeV/c, the reaction is not allowed by the nature of the simulation (or nature itself.)

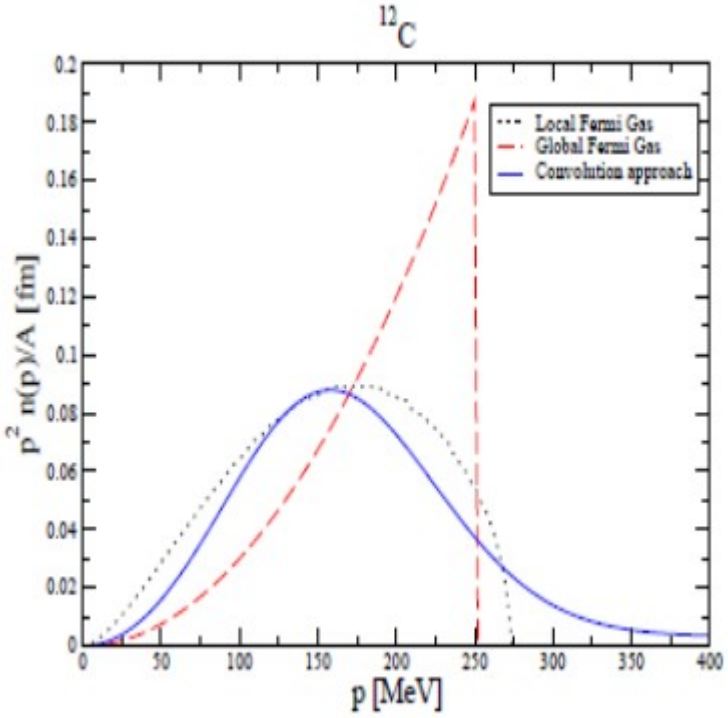

Figure 6: Three different approaches for modeling the momentum of the target nucleons. [2]

1.5 Candidate Model Additions

With evidence the MINERvA MC simulation does not have a complete model,

model adaptations or additions will have to be made. This analysis has two model additions to test, the Random Phase Approximation (RPA) and a meson exchange current (MEC) model. Several teams have developed models like these and used them to successfully describe electron-nucleus scattering. This work is focused on the ones developed by Juan Nieves, Manuel Vicente Vacas and collaborators at IFIC and the Universitat de Valencia, in Spain.[3][4]

To examine if our candidate models may make improvements to the disagreement between the MC and MINERvA data in figure 5, we will want to work with this q_0 and q_3 space. The contours of constant W continue as we increase the values of q_0 and q_3 to include other resonance production, coherent scattering, and deep inelastic scattering. Figure 7 is the same standard Genie model used to create the MINERvA MC, but now has contours of constant Q^2.

Routinely Q^2 is one quantity that is used to display and analyze particle physics data. Because it is a quantity that is the same in any reference frame (the nucleon, the neutrino, or the lab,) most scattering models are expressed as a function of this quantity. For the 2013 result as shown in Figure 1, the MINERvA team divided the sample into two regions of Q^2. This corresponds to the left-most white contour in Figure 7, which carves out an interesting route in our q_0 and q_3 space. If the analysis were to use Q^2 and q_0 as the MINERvA team used for Figure 1, we can see that Q^2 would include all types of neutrino scattering events. We will instead divide the space into regions of q_3 instead of Q^2 to the space, and thus the types of scattering events, that will make our sample.

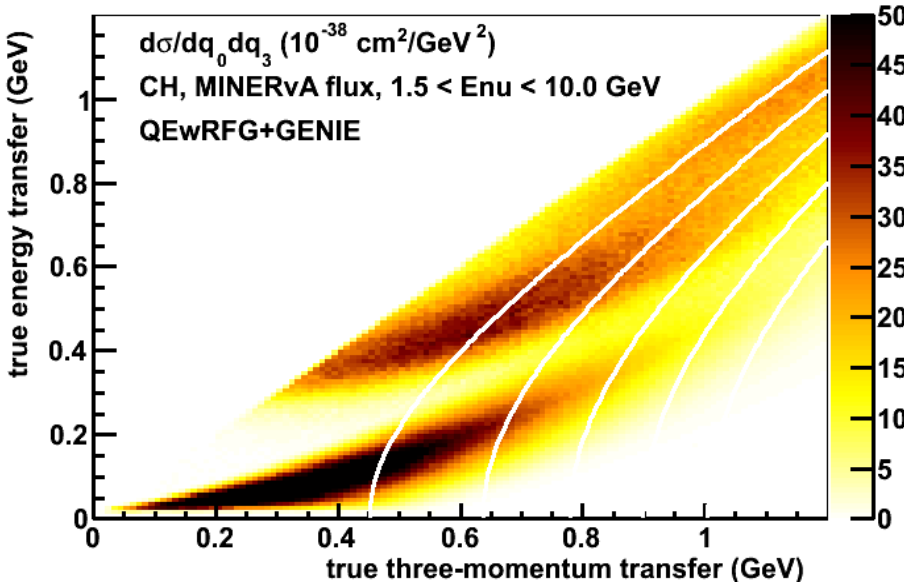

Figure 7: Intensity plot for the standard Genie double-differential cross section on carbon. Lines of increasing and constant Q^2 are shown from left to right

The ratio between the standard Genie model with the local Fermi gas model and the model with added RPA and MEC model additions will give an idea on where to look for the effects of RPA and MEC. Figure 8 shows the Genie model with the local Fermi gas and the RPA and MEC models added as well. As it is hard to see any difference between Fig. 8 and Fig. 5, so Fig. 9 is the ratio of the two, with the simple model of Fig. 5 in the denominator. The ratio plot shows red where events have been added between the standard genie model and our model with RPA and MEC added, and blue where events have been removed. The blue area at nearly zero energy transfer is a suppression of the cross section because of the RPA model. The red between the W contour for the QE process and delta resonance production is an enhancement of events from the MEC process.

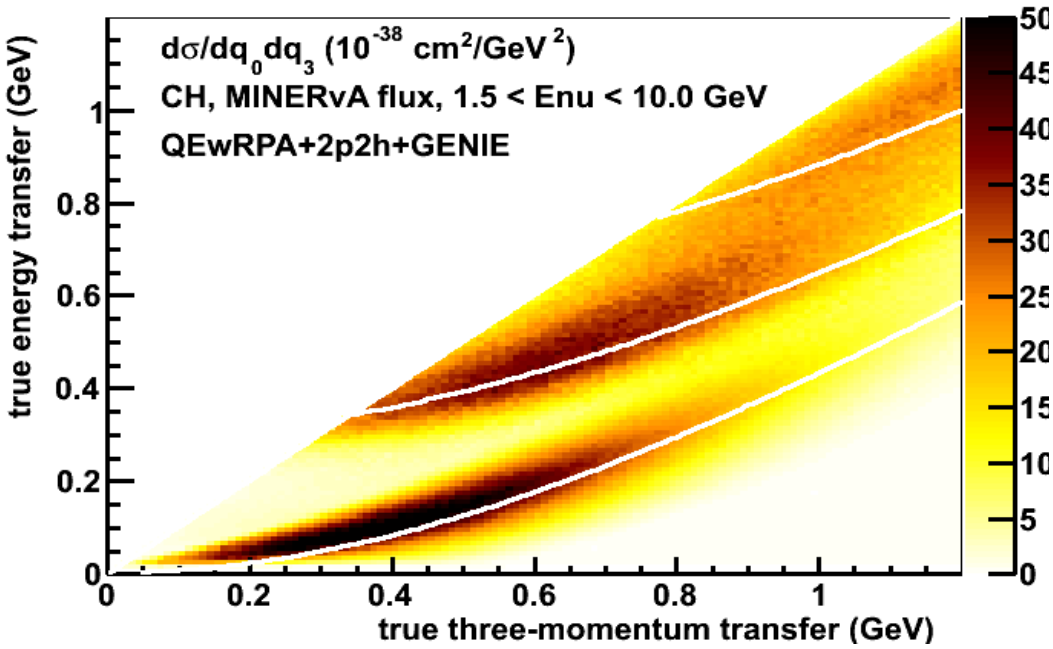

Figure 8: Intensity plot for the standard Genie double-differential cross section on carbon with the candidate RPA and MEC models included.

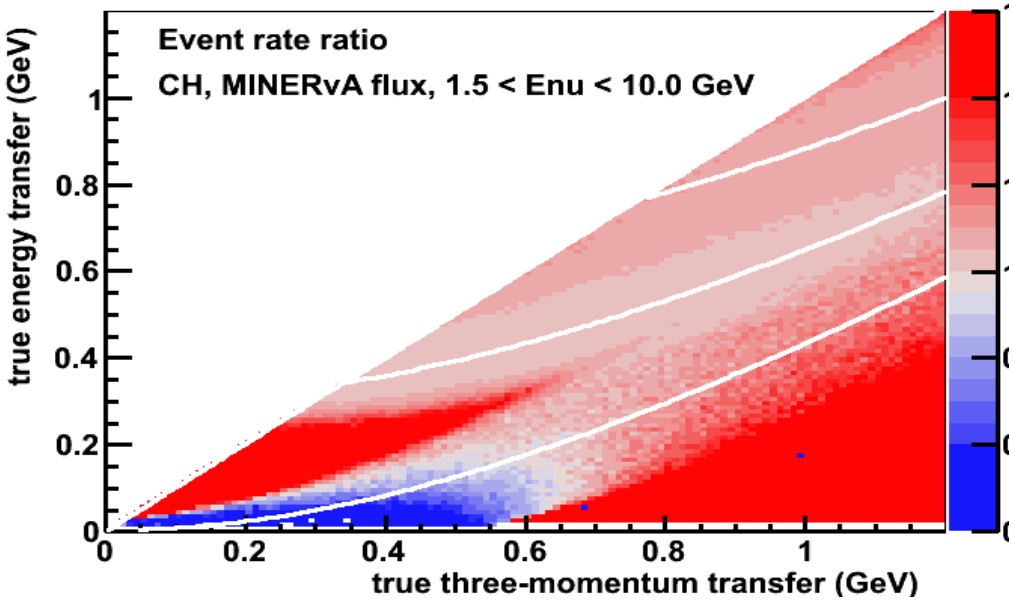

Figure 9: Plot of the ratio between the cross section for the Genie model with candidate RPA and MEC additions to the standard Genie model. Red corresponds to cross section enhancement while blue corresponds to cross section suppression

1.6 Random Phase Approximation (RPA) Model

The random phase approximation was developed in 1950s by David Bohm and David Pines.[5] It was originally developed to solve screening effects in an electron gas, important for modeling solid state systems. Perturbation and Hartree-Fock methods had fallen short at modeling long range electromagnetic effects in solid state physics. It is a collective effect of electrons in an electron gas to effectively screen and reduce the potential for other electromagnetic interactions with these electrons.

The random phase approximation also applies to the environment of the strong nuclear force and nucleons. The presence of a target neutron or proton is screened from the strong and weak forces, which lowers the ground state potential of the nucleus. The screening result also lowers the weak interaction scattering cross section, preferentially at values of low q_0. The prominent blue area at the bottom of Fig. 9 shows the predicted magnitude of this effect.

1.7 Meson Exchange Current Model

Meson exchange current (MEC) is a model for the scattering off multiple weakly bound nucleons. Nuclear interactions are mediated by the strong force. The strong force acts to hold quarks together using force mediators called gluons to produce hadronic particles. By extension, the strong force also binds protons and neutrons together in the nucleus. In quantum mechanics all forces are modeled by the exchange of an integer spin particles which are generically referred to as bosons. Between the pair of nucleons a virtual pion, consisting of a quark anti-quark pair,

is exchanged to bind the nucleus together. Quark and anti-quark pairs are generically referred to as mesons.

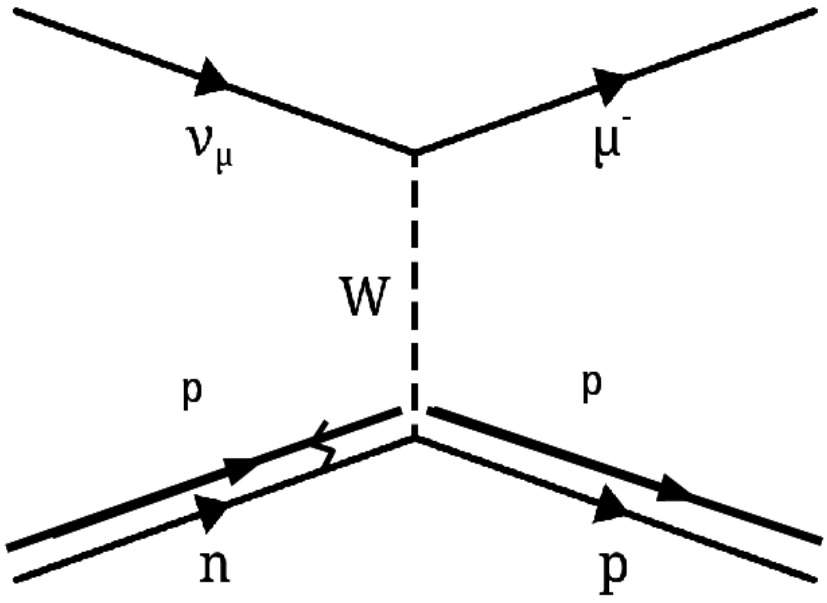

Figure 10: Feynman diagram for the meson exchange current scattering process. The incoming pn pair is bound by the exchange of a pion

With two nucleons bound, it is possible to scatter off of the bound nucleons, or effectively nucleons caught in the act of exchanging a pion. Figure 10 is a Feynman diagram for the meson exchange current. With a neutrino scattering off a proton and neutron pair the neutron is converted to a proton, and the neutrino becomes a muon. A neutrino can also scatter off a neutron and neutron pair producing a proton and neutron pair scattered from the nucleus.

When an outgoing neutron from this process is not observed in the detector, the reaction would appear to be a QE-like process. A delta resonance event where the pion was lost during a scatter as it exited the nucleus would also appear QE-like.

The 2013 MINERvA publication was analyzing a sample of QE-like events, and quantifying this discrepancy.

Meson exchange-current scattering is not currently part of the default Genie model for neutrino scattering but is necessary to properly model electron scattering. Electron scattering experiments had experienced similar discrepancy between their simulation and data until the MEC model was added. Although MEC scattering has never been observed for neutrino scattering most physicists assume it happens for neutrino scattering based on this electron scattering result. The MEC events will add to the cross section preferentially in the dip region between the peaks of QE and delta resonance production, as seen in figure 9.

1.8 Analysis Strategy

Our analysis will test systematic uncertainties in the standard Genie model and then test if adding the RPA and MEC models better describe the data. The decision to work with three-momentum transfer and energy transfer will allow us to cut our space into slices of three-momentum. For three-momentum less than 0.4 GeV, we can examine a slice in space where both the RPA and MEC models should have an effect. Figure 9 shows for this slice of three-momentum, which we will call low q_3, we will only have to consider QE and delta resonance production, without having to worry about higher resonance production, DIS, or coherent scattering events.

From the ratio plot figure 9, addition of the RPA model will affect QE events, and MEC events should be added at q_0 values between the QE peak and delta resonance peak.

Systematic uncertainty studies will confirm if changing parameters of the standard Genie model will not eliminate the data and MC discrepancies. Studies investigating delta production uncertainties, as well as resolution and biasing effects of the reconstruction of events in the detector are considered. Once these uncertainties have been checked the RPA and MEC models are added to Genie and we can gauge how the ratios improve. The systematic uncertainty studies are used to make error bands for the final plots.

Our analysis will utilize the eye-scanning of reconstructed events to search for multiple hadron, MEC like signatures. The adding of the MEC model predicts more events with two proton signatures. Using the MINERvA event viewer, Arachne,[6] it is possible to scan individual events for multiple hadron signatures. Scanning results for low q_3 could help strengthen the case that adding the MEC model is necessary.

2 The Detector

The Neutrinos at the Main Injector (NuMI) beam is important to modern neutrino physics experiments. The beam supports multiple neutrino scattering and neutrino oscillation experiments including MINERvA, NOvA, and MINOS. The beam was initially developed to study the parameters that describe neutrino oscillations. To determine these parameters, the mechanics of neutrino scattering must be understood with good precision. Original cross section measurements were made in spark and bubble chamber experiments. Some of the earliest examples include Kustan et al.[10] made in iron spark chamber measurements in 1969 and Mann et al. [11] in deuterium bubble chamber measurements in 1973. With the need for better cross section measurements and knowledge of the neutrino scattering processes, the MINERvA collaboration formed in 2004, and built a detector to use this beam. This analysis is from the first set of data taken, starting in 2010.

2.1 NuMI: The Production of Neutrinos

Protons are boosted through numerous stages to reach 120 GeV of energy in the main injector. The location and size of each stage are show in figure 11.[7] Protons start in the pre-accelerator at 770 keV. They pass down the linear accelerator Linac and reach 400 MeV. Next protons cycle the booster stage and reach 8 GeV before they are passed into the main accelerator and brought up to 120 GeV. At this energy neutrino beams with a flux peaking in the 2 GeV (MINERvA low energy data) or 6 GeV (MINERvA medium energy range) can be obtained.

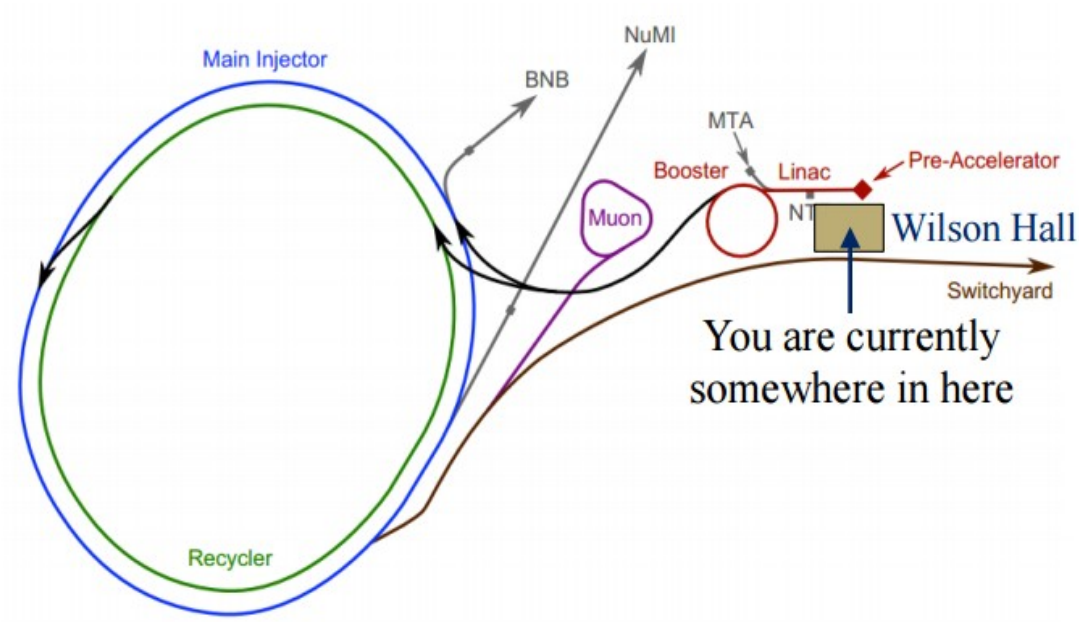

Figure 11: Diagram of the different accelerators that feed the main injector. You are currently somewhere in here, unless you are in Duluth or elsewhere reading this.[7]

Protons from the main injector are used to create kaons, pions, and other mesons which produce neutrinos from decay. Each spill from the main injector lasts 10 μs, and beam intensity is usually between $20x10^{12}$ and $35x10^{12}$ protons per spill. As of May 2015 beam intensity is $32x10^{12}$ protons per spill. These protons are sent at the NuMI beam's carbon target. The protons collide with the carbon target to produce mesons, primarily kaons and pions. For neutrino mode, the positively charged mesons are the important ones. Kaons will decay into a neutrino/anti-lepton partner or into more pions while pions decay into a neutrino/anti-lepton partner.

Two large magnetic horns focus the mesons produced at the target for travel through the decay pipe. The products of the proton collisions with the carbon target are scattered in all directions. The horns are tuned to focus only positively charged or only negatively charged products, which produce mostly neutrinos and anti-neutrinos respectively. The horn can also be tuned to change the energy peak

of the beam.

As the beam travels towards MINERvA, the hadronic absorber and dolomite rock remove unwanted particles from the beam. The remaining protons and mesons are absorbed in the hadronic absorber. The hadronic absorber removes only some of the muons produced from pion decay. There is roughly 240 meters of dolomite rock between the hadronic absorber and the MINERvA hall which prevents most muons from reaching the detector. The neutrino beam, which is now 98% pure muon neutrinos, is now ready pass through the MINERvA detector en route to Soudan (MINOS) and Ash River (NOvA) in Minnesota.

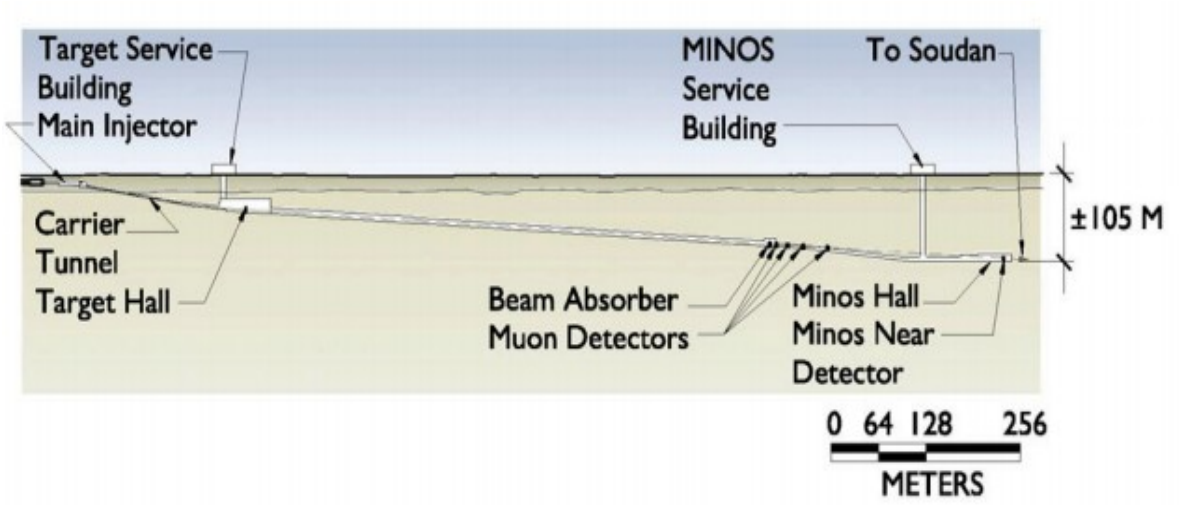

Figure 12: Schematic of the beam hall, from the main injector to the MINOS/MINERvA hall. The beam continues downstream to the Minos far detector

2.2 The MINERvA Detector

The MINERvA detector contains a veto wall, passive nuclear target region, an

active target and tracking region, side and downstream electromagnetic calorimeters (ecal) and hadronic calorimeters (hcal). In total, the MINERvA detector from the veto monitor through the back of the downstream hcal is 5.2 meters as seen in Fig. 13.[8] The MINOS detector is also used by MINERvA to track muons produced by neutrino scattering events, with the MINOS detector located 2 meters downstream of the MINERvA detector.

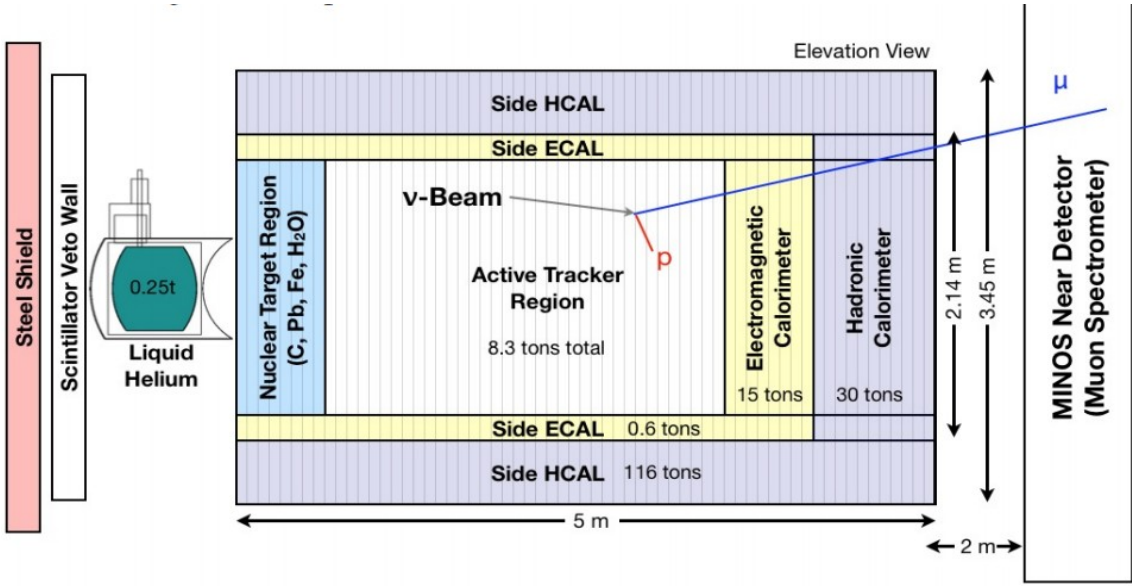

Figure 13: The MINERvA detector. The NuMI neutrino beam moves from left to right [8]

The MINERvA detector tracks particles by using scintillator. As a charged particle moves through the scintillator it deposits energy via the ionization of the material along its path. A scintillating molecule absorbs energy, and is kicked up into an excited quantum state. As the material relaxes towards lower energy states, photons are emitted and collected by optical fiber running through each scintillator strip, then read out by photomultiplier tubes. The number of photons collected is proportional to the energy deposited in the active scintillator. These energy values

require a passive material correction, which accounts for the energy lost traveling through passive, non-scintillator materials, including the epoxy and plastic that holds the scintillator planes together, and the lead and iron of the calorimeters.

Only charged particles are detected this way. Neutral particles (and the neutrinos themselves) are only detected when they interact and give energy to a charged particle. Neutrons can be considered lost energy in the detector, unless they decay or re-scatter and produce energetic charged particles. The neutral pion will decay into gamma ray photons which will re-scatter in the detector, producing a shower of electrons and positrons.

Inner detector scintillator strips are made of 1.7 cm tall by 3.3 cm wide triangles.[8] Strips are stacked together as shown in figure 14 where the red arrow illustrate a particle passing through two adjacent strips. Long triangular scintillator strips were chosen for the active tracking region for more precise reconstruction. Using triangular instead of rectangular strips produces two complementary, overlapping measurements, increasing the resolution of the particle location. The position of the particle is determined not just by which two strips are hit, but also by how the energy is shared between them.

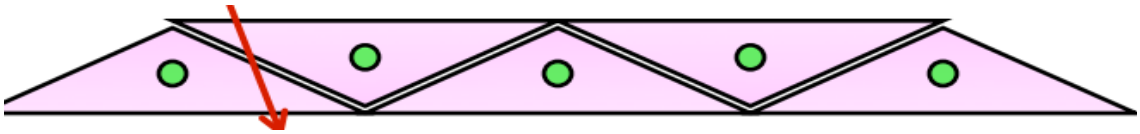

Figure 14: MINERvA inner detector scintillator construction. Triangles are 3.3 cm wide by 1.7 cm tall

Strips are assembled into planes, for which the MINERvA detector has three types. X planes define the transverse, horizontal axis of the detector, while U planes and V planes are rotated ± 60º and give the vertical position. Planes are arranged by

alternating X planes with a U or V plane, creating the pattern UXVX which is repeated. It is necessary to have more than one plane orientation so that a three dimensional reconstruction can take place. By having three different plane orientations instead of two the collaboration can be certain that along with accurately identifying the muon track that a separate hadron track could also be reconstructed unambiguously.

The veto wall is the most upstream component of the MINERvA detector. The veto wall can be used to identify and throw out events where muons passed into and through the detector. We are not using it for this analysis.

Next downstream is the target region. The target region contains scintillator with 6 planes of passive targets mixed in. Targets in this region include lead, iron, and water. Three of these targets are mixed lead and iron, one is stacked together as a carbon, lead, and iron mixture, and the last is a purely lead target. Downstream of these hanging targets there is also a kevlar bag filled with water. These targets are used for the analysis of cross section ratios for C/CH, Pb/CH, Fe/CH, and H_2O/CH but are not used for this analysis presented here.

Ecal and Hcal trackers make up the sides of the tracking region which we call the outer detector and importantly the last two downstream areas. The Ecal and Hcal are designed to be less precise in energy measurements than the active tracker region but effective at forcing more energetic particles to interact and leave their energy in the detector rather than passing out the back.

The Ecal is made of scintillator planes and lead. The high Z (charge) of the lead nuclei give electrons and gamma rays a much higher probability to re-interact via

bremsstrahlung and electron-positron pair production. This is vital for the detection of neutral pion energy. The neutral pions most common decay mode (99%) is to a pair of gamma rays. These, and also electrons, induce a compact and complete shower of energy in the Ecal.

The Hcal is made of active scintillator planes and passive planes of steel with a ratio of material of about 1:10. The Hcal is configured to sample energy of pions in a more coarse way than the inner detector tracker region. The benefit is that the steel is so dense that these pions and their products will rarely leave the sides or back of the detector. A coarse sampling of pion energy is better for accurate energy reconstruction than losing energy from a pion escaping the detector.

2.3 Generation of the Simulation (Monte Carlo)

Having a detailed simulation to compare to the detector data is vital for the physics analysis presented here. Steps are taken to ensure that the simulated events are created and reconstructed as similar as possible to data events. The MC simulation steps through multiple processes to ensure correct detector response so that the only differences should be between the model used for event generation in the MC and the true nature of the neutrino scattering events in the data. With this level of care we can explore if changing the parameters of the current model will fix the differences, or if model additions are necessary.

GENIE is used to simulate the scattering events, both the products of the initial reaction, and the final state interactions (FSI) as the products leave the target nucleus.[12] GENIE is based on standard neutrino scattering model elements, many tuned to previous neutrino and electron scattering data. A record of the kinematic

quantities is saved for all particles which exit the nucleus for each event. These “truth” quantities are also used for our analysis.

The next step is to simulate the final state particles after they leave the nucleus, which is done using Geant4.[13] Geant4 takes the energy and momentum vector of the final state particles from GENIE and simulates what their activity would look like in the detector. Energy loss, re-scattering and decay are simulated as the particles are stepped through the detector material.

The next step is to simulate the detector response. This means turning the energy losses into digitized amounts of activity associated with each scintillator strip. This is done with fluctuations in the detector response and calibrations that mimic the real detector.

Finally the simulation has all the properties of the data. The simulated events are treated by the same cleaning and reconstruction algorithms as the data. This last step produces the reconstructed kinematic quantities for the simulation, mimicking the way the data is processed. With a fully treated MC, reconstructed quantities between the data and MC should only possess differences between the GENIE model and nature.

This analysis uses MINERvA “Resurrection” processing of data and MC on the minerva1 and minerva13c playlists, which is two-thirds of the data from MINERvA's low energy running period. We are using genie version 2.6.2, which is the default version for “Resurrection” processing used from 2013 into 2015 and Geant4 version 9.4p2. We have also made a small fiducial cut to include only events that originate in the tracker region.

3 Eye Scanning of Events

The MEC process is predicted to often have two protons in the final state, which gives us an opportunity to scan events and look for direct evidence in neutrino scattering data. Based on the MINERvA test beam 1 run and Geant4 simulation, a proton in the MINERvA detector routinely deposits roughly 15-20 MeV of energy in the last strip of it's motion,[9] leading us to believe the short, forward going track in figure 15 is a proton. We can use our ability to view actual events to investigate the discrepancies and to look for signatures for our candidate MEC model in real data events. Scanning should also confirm trends that we see with the data analysis, namely that the MC overestimates in the lowest section of low q3 and underestimates in the dip region.

The MINERvA group has developed software for the viewing of reconstructed event display called Arachne.[6] Using the event run, sub run, gate, and slice information for the specific event Arachne displays the hit maps for the X, U and V views and includes truth information for MC events. We scanned for zero, one, and two+ hadron topologies in an attempt to classify multi-nucleon final states.

3.1 Scan Rules and Techniques

For scanning there were four types of hadron topologies that were counted. These types were tracks, stubs, vertex hits, and neutrons. For each event, we counted how many of each of these categories appeared. Then those results were reduced to three simpler classifications: zero hadrons, one hadron, or two or more hadrons. It is our goal to investigate the differences in the multi-hadron fraction between the data and MC in search of the MEC process.

The rules are in place to attempt to identify multiple hadron signatures and prevent

biasing in the results. Scanning of events in bubble chamber and spark chamber experiments were done with photographs of the reactions. In order not to bias the results, rules were put in place so the scanner would know exactly how to classify events. To prevent these biases in our results the scanners were given a robust set of instructions. In addition, some events were scanned by two or more people, and we evaluated consistency.

Arachne displays reconstructed events for each view with the color corresponding to the energy deposited. Figure 15 shows an X view with two tracks, at least one of which we've identified as a proton candidate. If the MEC process exists in nature we are hoping to see 2+ particle signatures that hint at additional protons.

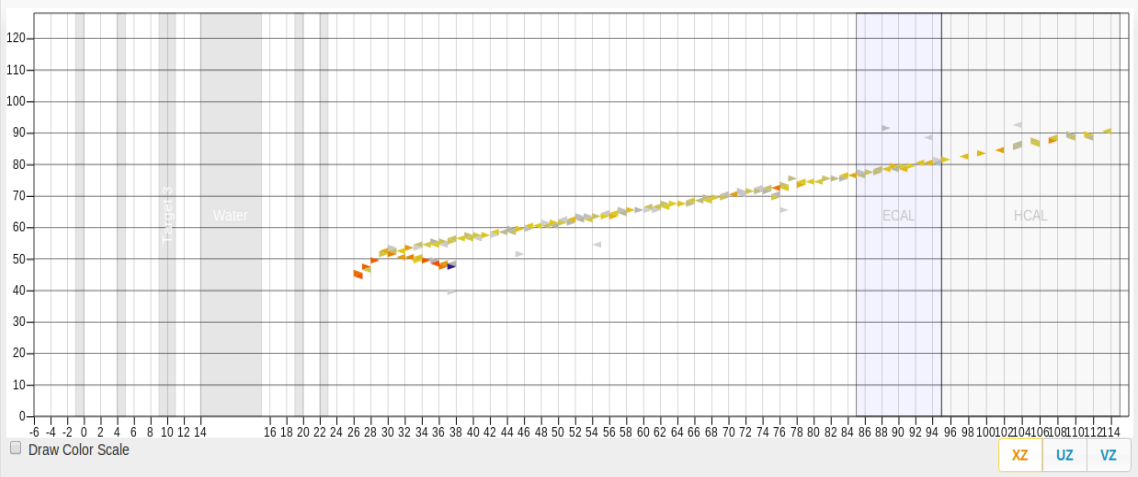

Figure 15: A scanned two track event. The downstream particle ending with a blue hit is a definite proton candidate, while the other track is more ambiguous.

It is necessary to define a unit length to describe distances from the vertex in order to classify stubs and tracks. A unit length in the direction of the beam is one plane, and a unit length perpendicular to the beam consists of one strip measured from the center of one strip to the next. In order to prevent the scanner from having to calculate lengths for hadrons that moved in both the strip and plane directions, the

distance traveled was assumed to be the sum of the strips and planes away from the vertex.

A track is a particle that travels five or more unit lengths from the vertex. There is no energy threshold for any hits along the track, just so long as the candidate particle has met the length requirement and can be traced back to the vertex of the scattering event. Figure 15 shows two short tracks coming from the vertex of the scattering event, with the muon produced representing the long track exiting the back of the detector downstream of the beam.

A stub is a particle that traveled 3 or 4 unit lengths from the vertex of the event. It is important that the particle path is traced back to the vertex of the event, and not from an interaction stemming from further down the muon track. There was no threshold energy set for the last hit on the stub. Figure 16 gives an example of a stub.

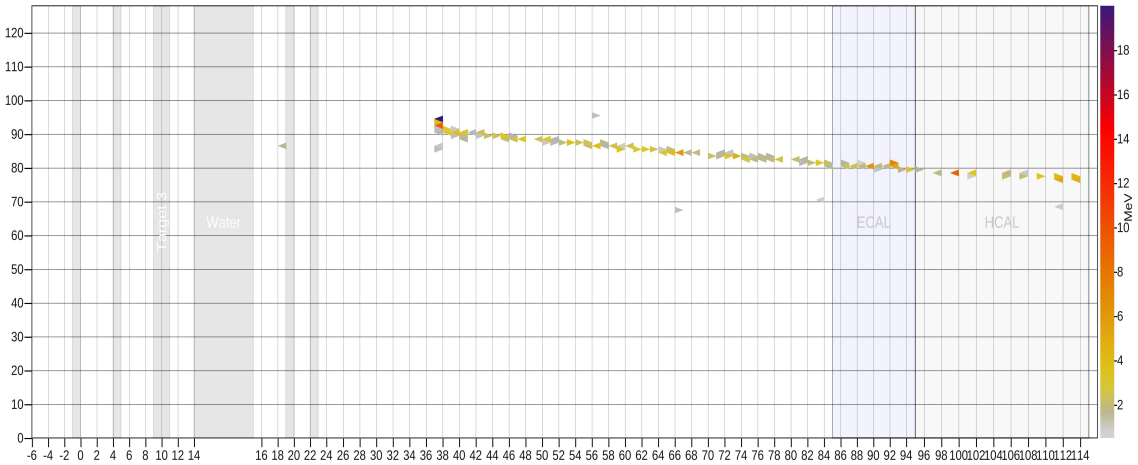

Figure 16: A stub event

A vertex hadron was counted for hits of 10+ MeV at the vertex, or within two unit lengths from the vertex. If two hits above the threshold energy shared adjacent

sides this was only counted as one vertex hit. If hits above the energy threshold were seen at the vertex in multiple views, each of these was counted as a separate vertex hadron since it is impossible to tell if they are from the same particle. Two vertex hadrons can occur in a single view if they are separated by one unit length with a hit less than 10 MeV. A vertex hadron could also be observed at the start of a stub or track.

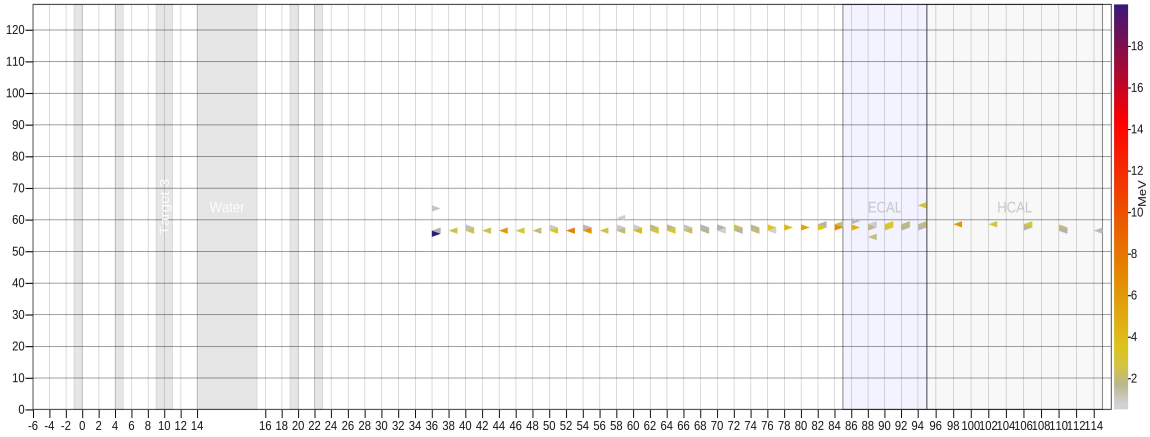

Figure 17: A single vertex hit

A neutron is classified as a hit away from the vertex with no discernible path from the vertex, and which visually could have originated from the vertex and not some other activity or the muon. These events were not used in any statistics, but were marked when seen. It is also possible that the scattering event did not have any of these, just the scattered muon produced.

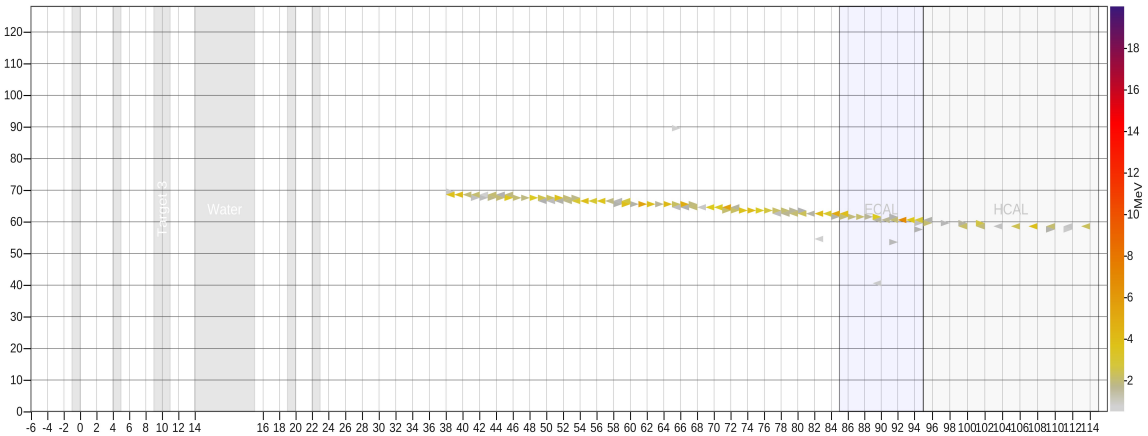

Figure 18: An uncategorized event. There are no vertex hits, stubs, or tracks

3.2 Double Scanned Data

The scan consisted of scanning 1100 unique MC events in the low q_3 region and double scanning 625 data events from the low q_3 region. The double scan originally occurred because of an error, but was beneficial in the end by providing a self check of the consistency of the scan rules. Only 25 events from the double scanned data sets were done by the same person, meaning that the double scan was predominately two different sets of eyes on each event.

With the scans complete and ready for analysis, it is useful to look at the distributions of hadrons in the entire low q_3 sample, but to also divide the low q_3 sample into regions of recoil energy, to isolate the dip region. Using our new version of recoil energy, energy in the tracker, we can break the low q_3 into three regions of interest. Low tracker-energy is less than 0.04 GeV and corresponds to the QE peak where the MC overestimates the data and where we expect to find the RPA suppression effect. Mid tracker-energy is between 0.04 GeV and 0.14 GeV and corresponds to the dip region where the MC underestimates the data. This is the region where the MEC model may play the most visible role in the low q_3

region, so this is of special interest. The last region is high tracker-energy with energies between 0.14 GeV and 0.25 GeV, which is the maximum possible energy in the tracker for the low q_3 cut. We expect this region to be dominated by delta resonance production. Scan results from these different regions will be highlighted.

The double scanned data allowed us to check if the scanners can consistency follow the scanning rules. Of the 625 data events that were scanned there were 148 total events in which the scanners disagreed (23.7%). Ethan and I went through each of these events and agreed upon a final classification of each of these events. After rationalizing the data scan there were 38 events in which neither of the scanners original scan matched with the rationalized scan. The calculated uncertainties are the binomial statistical uncertainty. Table 1 contains the two separate data scans with the rationalized corrected data scan on the far right.

q0_tracker	**Data 1**		**q0_tracker**	**Data 2**		**q0_tracker**	**Corrected Data**		
Data1 high tracker	80	percentage	Data 2 high tracker	80	percentage	high q0_tracker	80	percentage	Uncertainty %
0 hadrons	0	0.00	0 hadrons	0	0	0 hadrons	0	0	
1 hadron	16	20.00	1 hadron	19	23.75	1 hadron	16	20	4.5
2+ hadrons no track/stub	4	5.00	2+ hadrons no track/stub	16	20	2+ no track	12	15	4.6*
2+ hadrons w track/stub	59	73.75	2+ hadrons w track/stub	42	52.50	2+ with track	51	63.75	4.6*
not available	1	1.25	not available	3	3.75	not available	1	1.25	
Data 1 mid tracker	306	percentage	Data 2 mid tracker	306	percentage	mid q0_tracker	306	percentage	Uncertainty %
0 hadrons	20	6.54	0 hadrons	13	4.25	0 hadrons	18	5.88	1.3
1 hadron	168	54.90	1 hadron	181	59.15	1 hadron	175	57.19	2.8
2+ hadrons no track/stub	50	16.34	2+ hadrons no track/stub	61	19.93	2+ no track	56	18.30	2.8*
2+ hadrons w track/stub	68	22.22	2+ hadrons w track/stub	50	16.34	2+ with track	56	18.30	2.8*
not available	0	0.00	not available	1	0.33	not available	1	0.33	
Data 1 low tracker	239	percentage	Data 2 low tracker	239	percentage	low q0_tracker	239	percentage	Uncertainty %
0 hadrons	131	54.81	0 hadrons	128	53.56	0 hadrons	129	53.97	3.2
1 hadron	105	43.93	1 hadron	105	43.93	1 hadron	105	43.93	3.2
2+ hadrons no track/stub	2	0.84	2+ hadrons no track/stub	4	1.67	2+ no track	3	1.26	0.7*
2+ hadrons w track/stub	1	0.42	2+ hadrons w track/stub	0	0.00	2+ with track	0	0.00	
not available	0	0.00	not available	2	0.84	not available	2	0.84	
Data1 tracker total	625	percentage	Data 2 tracker total	625	percentage	total	625	percentage	Uncertainty %
0 hadrons	151	24.16	0 hadrons	141	22.56	0 hadron	147	23.52	1.7
1 hadron	289	46.24	1 hadron	305	48.8	1 hadron	296	47.36	2
2+ hadrons no track/stub	56	8.96	2+ hadrons no track/stub	81	12.96	2+ no track	71	11.36	1.8*
2+ hadrons w track/stub	128	20.48	2+ hadrons w track/stub	92	14.72	2+ with track	107	17.12	1.8*
not available	1	0.16	not available	6	0.96	not available	4	0.64	

Table 1: Results from double scanning 625 data events. The disagreements between the first two columns are rationalized and create the third column

Disagreements between the scanners were corrected between both sets. Frequently the discrepancies between the two scanned sets differed not on total hadrons counted, but in the classification of tracks and stubs. For these events, one of the two scanners had correctly classified the event the same as the rationalized result. Much less frequently both scanners had miscounted the number of hadrons used in the final rationalized scan. These are the 38 events neither scanner agreed with the rationalized scan. These errors usually occurred when there was lots of activity which lead to difficulty counting vertex hadrons.

3.3 MC and Data Scan Comparison

With a rationalized data scan we can compare the MC scan and data scan side by side. Table 2 contains the MC scanned results on the left column and the corrected data in the right column. Each column contains the results for the total low q_3 sample in the bottom row. The the results from each recoil energy section are the top three rows, starting with high tracker-energy at the top of the table.

q0_tracker	MC Scanned			q0_tracker	Corrected Data		
High tracker total	160	percentage	uncertainty	high q0_tracker	80	percentage	Uncertainty %
0 hadrons	9	5.63	1.8	0 hadrons	0	0	
1 hadron	43	26.88	3.5	1 hadron	16	20	4.5
2+ hadrons no track/stub	15	9.38	3.7*	2+ no track	12	15	4.6*
2+ hadrons w track/stub	93	58.13	3.7*	2+ with track	51	63.75	4.6*
not available	0	0.00		not available	1	1.25	
med tracker total	372	percentage	uncertainty	mid q0_tracker	306	percentage	Uncertainty %
0 hadrons	42	11.29	1.6	0 hadrons	18	5.88	1.3
1 hadron	204	54.84	2.6	1 hadron	175	57.19	2.8
2+ hadrons no track/stub	48	12.90	2.4*	2+ no track	56	18.30	2.8*
2+ hadrons w track/stub	77	20.70	2.4*	2+ with track	56	18.30	2.8*
not available	1	0.27		not available	1	0.33	
low tracker total	568	percentage	uncertainty	low q0_tracker	239	percentage	Uncertainty %
0 hadrons	332	58.45	2.7	0 hadrons	129	53.97	3.2
1 hadron	232	40.85	2.1	1 hadron	105	43.93	3.2
2+ hadrons no track/stub	3	0.53	.3*	2+ no track	3	1.26	0.7
2+ hadrons w track/stub	0	0.00	.3*	2+ with track	0	0.00	
not available	1	0.18		not available	2	0.84	
tracker total	1100	percentage	uncertainty	total	625	percentage	Uncertainty %
0 hadrons	383	34.82	1.4	0 hadron	147	23.52	1.7
1 hadron	479	43.55	1.5	1 hadron	296	47.36	2
2+ hadrons no track/stub	66	6.00	1.2*	2+ no track	71	11.36	1.8*
2+ hadrons w track/stub	170	15.45	1.2*	2+ with track	107	17.12	1.8*
not available	2	0.18		not available	4	0.64	

Table 2: The final MC scan results with the rationalized data scan results. Total numbers for the entire q_3 region in the bottom row, with results from each tracker-energy section above

MC and data scans show discrepancies between the MC and data sets which are similar to our low q_3 histogram. Focusing on the bottom row total, the MC has more 0 hadron events than the data, and less 2+ hadrons. These results hold up when looking into each section of tracker-energy. In the high tracker region the MC has underestimated the number of 2+ hadron events by roughly 11%. In the low tracker region the MC has overestimated the number of 0 hadron events by 11%. Interestingly, these effects are also seen in the mid tracker region, which has special importance because of the MEC models prediction of events in this region.

3.4 MC Scan Truth Comparison

With the MC scan, we can also check how accurate the scan was to the truth information for each event. Table 3 contains the distribution of protons and charged pions with energy above 10 MeV. The # match column represents how many events were scanned to match the truth particle given that number of truth particles. For the 1100 MC events scanned there were 667 events (60.6%) for which the truth number of particles matched.

q0_tracker Truth 10 MeV

high q0	160	percentage	# match	percentage match
0 hits	0	0.00	0	
1 hit	57	35.63	33	57.89
2+ hits	103	64.38	37	35.92
not available	0	0.00	0	

med q0	372	percentage	# match	percentage match
0 hits	21	5.65	17	80.95
1 hit	247	66.40	164	66.40
2+ hits	103	27.69	34	33.01
not available	1	0.27	0	

low q0	568	percentage	# match	percentage match
0 hits	200	35.21	189	94.5
1 hit	334	58.80	192	57.49
2+ hits	33	5.81	1	3.03
not available	1	0.18		

total	1100	percentage	# match	percentage
0 hits	221	20.09	206	93.21
1 hit	638	58.00	389	60.97
2+ hits	239	21.73	72	30.13
not available	2	0.18		

Table 3: The number of hadrons by truth particle. The number matching and percent matched correspond to scans that had the same number of hadrons

Matching the MC truth with a scan was much more successful for lower energy and lower hadron events. In the low tracker region (denoted low q_0 in table 3) there were 382 events out of 568 for a 67 percent match. This percentage decreases through the mid tracker region to nearly 58% and reaches 44% in the high tracker region. As we can see in the totals for the low q_3 region the matching efficiency of the scan decreased as the number of hadrons increased. The MC scan was 93% efficient for 0 hadron truth events, 61% for 1 hadron truth events, and

30% for 2+ hadron events. There is a threshold to identify a hadron, so the zero hadron events are usually correct.

3.5 Preliminary Scanning Results

Comparing the scanning results for the 1100 MC events and 625 data events mirrors the trend that we see in our low q_3 distribution. When looking over the entire low q_3 sample, we see that the MC has an excess of zero hadron topologies, and a lack of 2+ hadron topologies compared to data. This would suggest that removing zero hadron events and adding 2+ hadron events to the MC would improve the discrepancies seen in scanning.

Our candidate models, RPA and MEC would weight down low energy QE events and add in more multi-particle events. The RPA would take effect in the low tracker-energy region, weighting down 0 hadron events in table two which would increase the percentage of 1 and 2 hit events. The MEC process could contribute to all three of these tracker-energy sections, but would be emphasized in the mid tracker-energy dip region as the QE events tail off and delta events have not reached their peak production in this section of q_3

3.6 Number of Hits Algorithm

In an attempt to count the number of hadrons per event to achieve higher statistic results without physically scanning we turned to algorithmically count the number of hadrons. We already had a quantity in our ntuple we thought may work, the number of hits over 10 MeV. The 10 MeV value corresponds to our energy cutoff for what was defined as a vertex hit. Exploiting the proton depositing 15-20 MeV

of energy in the last slices in its travel led us to believe the number of hits over 10 MeV may be a way to count protons.

Data Hits above 10 MeV			
Mid q0_tracker	731	percentage	uncertainty
0 hits	47	6.4	0.9
1 hit	258	35.3	1.8
2+ hits	426	58.3	1.8

MC Hits above 10 MeV			
mid q0_tracker	7726	percentage	uncertainty
0 hits	762	9.86	0.34
1 hit	2906	37.61	0.55
2+ hits	4058	52.52	0.57

MC Scanned			
med tracker total	372	percentage	uncertainty
0 hadrons	42	11.29	1.6
1 hadron	204	54.84	2.6
2+ hadrons no track/stub	48	12.9	2.4*
2+ hadrons w track/stub	77	20.7	2.4*
not available	1	0.27	

Table 4: Results for data hits over 10 MeV, MC hits over 10 MeV, and the MC scanning results

Listed are the results for nhits for both data and MC with the scanned MC results for the mid tracker-energy region. Comparing the nhits algorithm to the scanned MC shows that nhits above 10 MeV are similar to the scanned results. There may be a correlation between these values, which is promising. The MC nhits compares well to the scanned MC set shown in column three of table 4 for the 0 hits category. The 1 hit and 2+ hits categories are not direct matches, but if this algorithmic approach appears robust it is possible a “confusion matrix” could sort out the mix between 1 hadron and 2+ hadron cases and provide an avenue for the algorithmic scanning approach to work.

Comparing the MC nhits results to the data nhits results shows the same trend as the scanning results. The MC has an excess of 0 hit events and a deficit of 2+ hits events in the mid tracker-energy region. This result somewhat matches the results for scanning in the mid tracker-energy region and matches the results of the entire low q_3 region.

Since nhits over 10 MeV may work as a counting algorithm we should take a closer look at the average number of nhits for different truth processes within our sample. Using truth particle number information and the nhits algorithm, we can

determine the average number of hits over 10 MeV for different types of events. Events were selected in five categories, 1 truth proton only, 2 protons only, 1 pion and 1 neutron, 1 pion only, and 1 neutron only. These categories were selected to mimic the normal final states of the QE and delta resonance production. Nhits stats were done for each of these types of events and are listed below in table 5 along with the average number of hits for the certain type of event in the mid tracker-energy region.

Mid q0_tracker only	7726	Total Events									
nhits											
	1 Proton Only	3313	Percentage		2 Protons Only	192	Percentage		1 Pion only	700	Percentage
	0 hits above 10	187	5.6		0 hits above 10	1	0.5		0 hits above 10	107	15.3
	1 hit above 10	1574	47.5		1 hit above 10	113	58.9		1 hit above 10	265	37.9
	2 hits above 10	1021	30.8		2 hits above 10	63	32.8		2 hits above 10	198	28.3
	3+hits above 10	531	16		3+ hits above 10	15	7.8		3+ hits above 10	130	18.6
		Average	1.63			Average	1.52			Average	1.59
	1 Pion + 1 Neutron	466	Percentage		1 Neutron	190	Percentage				
	0 hits above 10	32	6.9		0 hits above 10	113	59.5				
	1 hit above 10	151	32.4		1 hit above 10	51	26.8				
	2 hits above 10	158	33.9		2 hits above 10	20	10.5				
	3+hits above 10	125	26.8		3+hits above 10	6	3.2				
		Average	1.92			Average	0.58				
	4861	Events	63.00%	Of Total							

Table 5: Results for nhits counting for specific events in the mid tracker-energy region. Final states were chosen to represent final states of QE and delta resonance processes

The success of the scanning algorithm depends on distinguishing between these different types of final states. The average number of hits is one distinguishing factor. We want the algorithm to categorize 1 proton, 2 proton, and pion events differently because they follow the interesting processes for which we're trying to distinguish between such as QE, MEC and delta events. If it works we can get an idea of how often these occur in the data differently than the MC.

The results for one proton show an average of 1.63 hits over 10 MeV, which makes sense knowing most protons deposit 15-20 MeV in the last few strips of its motion. Conversely 1 neutron events show 0.58 average hits over 10 MeV.

Neutrons do not deposit energy in the detector as they move since they are uncharged, which leads to this effect. We also see that the average for 1 pion and 1 neutron events is roughly the same as adding the individual results for 1 pion and 1 neutron.

Distinguishing between neutrons and pions works, but there are issues with 1 proton, 2 proton, and 1 pion events. With the nhits algorithm the average number of hits for 2 proton events is lower than 1 proton only events at 1.52 hits and 1.63 hits respectively. 1 pion events also produced a similar average of hits at 1.59 hits. With these events registering the same average number of hits per event, it is not possible to separate proton candidates from pion candidates using this counting method.

3.7 Number of Hits Near the Vertex

Looking in a vertex region could help the algorithm by distinguishing between hadrons that preferentially leave the vertex, and hadrons that stay in the vertex region. This could change our results for protons and pions and provide a more robust scanning algorithm. Nhits over 10 MeV in the vertex region is the result of drawing a rectangle around the vertex region. The rectangle is 5 strips and 5 planes on either side of the determined vertex.

With our new vertex definition the same trends exist between the MC and data. On the left are the nhits vertex distributions for MC and data, followed on the right by the original nhits distributions. As expected, the transition to the vertex nhits shifts the events into lower hit totals as some hits are now outside of the vertex region and are not counted.

MC Hits above 10 MeV VTX			
mid q0_tracke	7342	percentage	uncertainty
0 hits	1254	17.1	0.44
1 hit	2955	40.2	0.57
2+ hits	3133	42.7	0.58

MC Hits above 10 MeV			
mid q0_tracke	7726	percentage	uncertainty
0 hits	762	9.86	0.34
1 hit	2906	37.61	0.55
2+ hits	4058	52.52	0.57

Data Hits above 10 MeV VTX			
Mid q0_tracke	749	percentage	uncertainty
0 hits	79	10.5	1.1
1 hit	292	39	1.8
2+ hits	378	50.5	1.8

Data Hits above 10 MeV			
Mid q0_tracke	731	percentage	uncertainty
0 hits	47	6.4	0.9
1 hit	258	35.3	1.8
2+ hits	426	58.3	1.8

Table 6: A comparison between nhits and nhits vertex for both the MC and data. The right column results are repeated from table 4

As before we'd like to examine if the vertex definition changed our average number of hits for different truth events. Really, we are looking for a distinction between 1 proton and 2 proton signatures so that an algorithm can distinguish between the two sets. The results are listed in table 7.

The average nhits for 1 pion, 1 pion and 1 neutron, and 1 neutron all decrease. As we expected these types of hadrons are preferentially leaving the vertex region. Energetic pions thus are able to easily exit the vertex region. 1 pion events drop from an average of 1.59 in table 5 to 0.86 with the vertex definition in table 7. Neutrons decrease from 0.58 to 0.18 and the total for 1 pion 1 neutron events

Unfortunately changing to a vertex counting of 10 MeV hits does not resolve our 1 proton and 2 proton signature issue. We find that the average hits for 1 proton is 1.58 hits, while the average hits for 2 protons is 1.52 hits. The vertex definition did not change these enough to distinguish between one and two proton events, actually bringing the averages closer together. This does not provide an answer of

why one proton and two proton events look so much alike in the simulation.

Mid q0_track nhits_vtx	**7342**											
	1 Proton Onl	**3132**	**Percentage**	**Uncertainty**	**2 Protons On**	**192**	**Percentage**	**Uncertainty**	**1 Pion only**	**655**	**Percentage**	**Uncertainty**
	0 hits above	201	6.4	0.4	0 hits above	1	0.5	0.5	0 hits above	307	46.9	2.0
	1 hit above 1	1516	48.4	0.9	1 hit above 1	113	58.9	3.6	1 hit above 1	202	30.8	1.8
	2 hits above	955	30.5	0.8	2 hits above	63	32.8	3.4	2 hits above	103	15.7	1.4
	3+ hits above	460	14.7	0.6	3+ hits above	15	7.8	1.9	3+ hits above	43	6.6	1.0
		Average	**1.58**			**Average**	**1.52**			**Average**	**0.86**	
	1 Pion + 1 Ne	**446**	**Percentage**	**Uncertainty**	**1 Neutron**	**180**	**Percentage**	**Uncertainty**				
	0 hits above	130	29.1	2.2	0 hits above	153	85	2.7				
	1 hit above 1	204	45.7	2.4	1 hit above 1	24	13.3	2.5				
	2 hits above	81	18.2	1.8	2 hits above	2	1.1	0.8				
	3+ hits above	31	7.0	1.2	3+ hits above	1	0.6	0.6				
		Average	**1.06**			**Average**	**0.18**					
	4605	**Events**	**62.70%**	**Of Total Mid q0**								

Table 7: The hits breakdown and average number of hits for our vertex definition. Events with neutrons and pions saw major decreases in average number of hits

3.8 Two Proton Events, Energy Sharing

Two proton events produce 1 hit topologies and fewer 2 hit because the protons have such low energy they cannot leave the strip in which the neutrino interaction occurred. With the issue of 1 proton and 2 proton signatures still persisting with our nhits vertex algorithm we decided to quantify how 2 proton final states shared energy in the standard Genie model. The Nieves MEC model currently assumes the two nucleons scattering will share equal energy in the center of mass frame. By investigating the truth energy for the two protons we can check to see if they are tending to share energy equally.

If the two protons are sharing energy very equally, it could help to explain why two protons looks identical to one proton using the number of 10 MeV hits as a scanning algorithm. In contrast if the protons are unequally sharing the energy this could produce a hit at the vertex and a hit away from the vertex. Since we are not yet simulating MEC processes, these 2-proton events are our closest example in

GENIE.

Two proton events sharing equal energies leave less hits, while two proton events with unequal energies have more hits. To analyze how the two proton events were sharing energy, we used our MC set to list the two most energetic protons and calculated the energy of the most energetic proton over the total energy of the two protons. Figure 19 below shows the results. The average first proton energy percentage was 64.6%. With this result, it seems as if the two proton events are being similar to what we expect from the Nieves result which is that these protons should share energy equally more often than not. As a check we took all of the events above and below the average proton energy sharing % and calculated the average number of vertex hits. Events above the average of 64.6% for leading proton energy percentage produced 1.69 hits per events, and events below the average produced 1.38 hits per event. This result is opposite of what our initial hypothesis was, that the 1 proton and 2 proton events have the same average number of hits because because the two protons are not equally sharing energies.

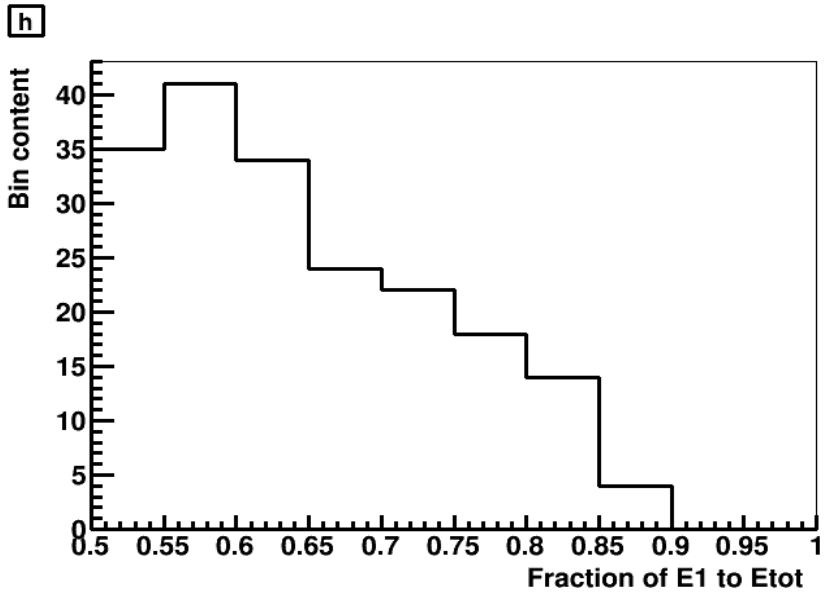

Figure 19: The percentage of energy of the most energetic proton for two proton events

3.9 RPA Weighted Nhits

With the trends between the MC and data holding for scanning and both of the number of hits algorithmic approaches it seems as if the addition of the RPA reweight would be a welcomed addition to our model. Our last algorithm test involved turning on the RPA effect to see if it alone could account for the discrepancy between counting the number of hits for MC and data. Instead of counting each event with an equal weight of 1, events were counted using the RPA weight associated with the event.

When the RPA weight is applied we see the percentages in the MC makes up some of the margin of the original discrepancy. MC 0 hits in the mid tracker-energy region decreases from 17.1% to 15.7% and the 2+ hits category increases from 42.7% to 45.3%. Both of these gains are in the correct direction to reconcile the MC and data.

These trends are also apparent not just in the mid energy in the tracker region, but throughout our entire low q_3 sample. Table 9 shows the 0 hits events decrease from 41% to 34.8% with the RPA weight added while 2+ hit events increase from 23.8% to 29.2%.

MC nhits VTX w RPA		
mid q0	6662.48	percentage
0 hits	1048.67	15.74
1 hit	2593.85	38.93
2+ hits	3019.96	45.33

7342 # of events

Data Hits above 10 MeV VTX		
Mid q0_tracke	749	percentage
0 hits	79	10.5
1 hit	292	39
2+ hits	378	50.5

MC Hits above 10 MeV VTX		
mid q0_tracke	7342	percentage
0 hits	1254	17.1
1 hit	2955	40.2
2+ hits	3133	42.7

Table 8: Mid tracker-energy (the dip region) nhits vertex with the RPA weight added

MC nhits VTX w RPA		
low q3	15919.08	percentage
0 hits	5538.23	34.79
1 hit	5725.49	35.97
2+ hits	4655.36	29.24

Data Hits above 10 MeV VTX		
low q3	1552	percentage
0 hits	455	29.3
1 hit	561	36.1
2+ hits	536	34.5

MC Hits above 10 MeV VTX		
Low q3	20123	percentage
0 hits	8256	41.03
1 hit	7073	35.15
2+ hits	4794	23.83

20123 # of events

Table 9: Nhits vertex with the RPA weight added for the entire low q_3 sample

Adding MEC events would not produce the required change to fully close the nhits vertex discrepancy between data and MC, but reducing pions could. Reducing the amount of pions would shift a higher percentage of events into the 2+ hits category based on the results from table 7. This would continue to improve the 0 hits/2+ hits discrepancy between the data and MC.

3.10 Scanning Results

With the original scan of 625 data events and 1100 MC events we determined that the MC had an excess of 0 hadron signatures and a deficit of 2+ hadron signatures. This trend was consistent in our three different sections of low q_3; low, mid, and high energy in the tracker region. With the possibility of MEC events populating the mid energy in the tracker region which is between the QE and delta resonance production peaks an algorithmic scanning approach was explored.

Both algorithmic approaches counted the number of hit slices above 10 MeV in the detector, with one approach just counting hits in a vertex region. Both algorithms mirrored the same trends, but upon trying to classify event types by the number of hits both algorithms failed at differentiating between 1 proton and 2 proton events. After investigating why 2 proton events may look like 1 proton events the conclusion is that number of hits over 10 MeV will not work as an algorithm designed to scan for proton multiplicity.

Since the trends between the MC and data were the same for scanning events and the two different algorithmic approaches we decided to apply the RPA reweight to see what effect it had on our percentages. In both the mid tracker-energy region and the entire low q3 sample the RPA reweight made positive gains in reconciling the differences between MC and data distributions, although it was not enough to make up the total difference alone. This gives direct evidence that the RPA reweight is a helpful addition to our Genie model, but does not make up the entire discrepancy as if further model tweaks are also necessary.

3.11 Delta Scanning

Further scanning studies were completed to examine the differences between the MC delta simulation and the delta component of the data. Figure 2 shows the ratio between data and MC dips below 1 at an energy in the tracker + ecal value of 0.2 GeV. Since the delta produces events with and without a pion, and since one MEC component (not in the MC) produces events without pions, we can ask whether the the fractional pion content of this region is predicted, or if the MC has too many pions. Scan rules were put into place to identify the pion content of the delta section of low q_3 by examining events with energy in the tracker + ecal greater than 0.14 GeV.

Four types of topologies were tracked in an attempt to separate pion events from non-pion events. These topologies were a uniform track, an increasing track, a track with decay or debris, and other. The uniform track and track with debris or decay categories are assumed to be mostly pions while an increasing track mostly protons. The “other” category we assume to be a healthy mix of both protons and

pions, and was used as a catch-all for events that could not be classified as one of the previous three event definitions.

A uniform track is a track leaving the vertex region in which there is not an increase of energy deposited at the end of the track. The vertex region is defined by drawing a 10 plane by 10 strip box with the vertex of the event in the center of the box. Figure 20 shows an example of a uniform track.

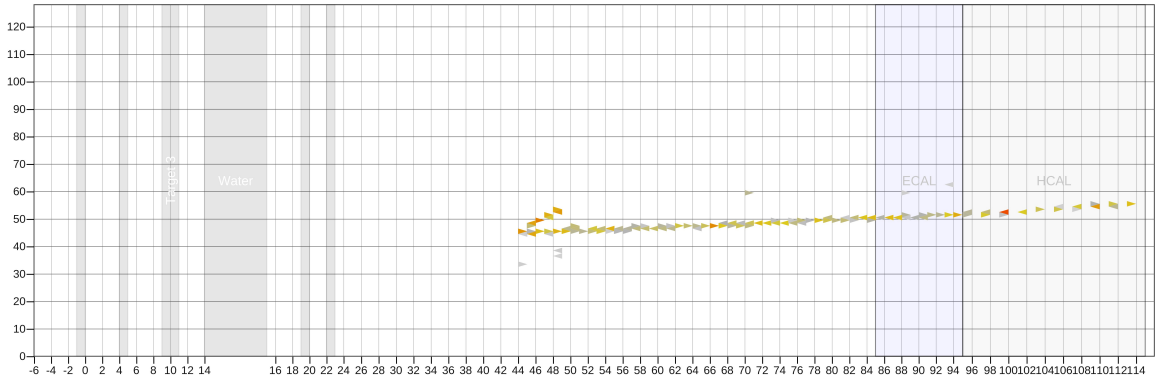

Figure 20: A uniform track

A track with increasingly large energy deposits, an “increasing track”, leaves the vertex region and ends with one or more hits greater than 20 MeV. The 20 MeV limit was set in place to identify proton candidates. Heavier charged particles (protons with 938 MeV/c^2 in this case, but deuterons and alpha particles also) deposit their last 30 to 50 MeV of energy in a shorter distance than lighter charged particles such as pions and electrons. This characteristic is often exploited by particle identification algorithms to separate protons from other species, and is what we're asking the eye-scanners to do. Figure 21 shows an increasing track.

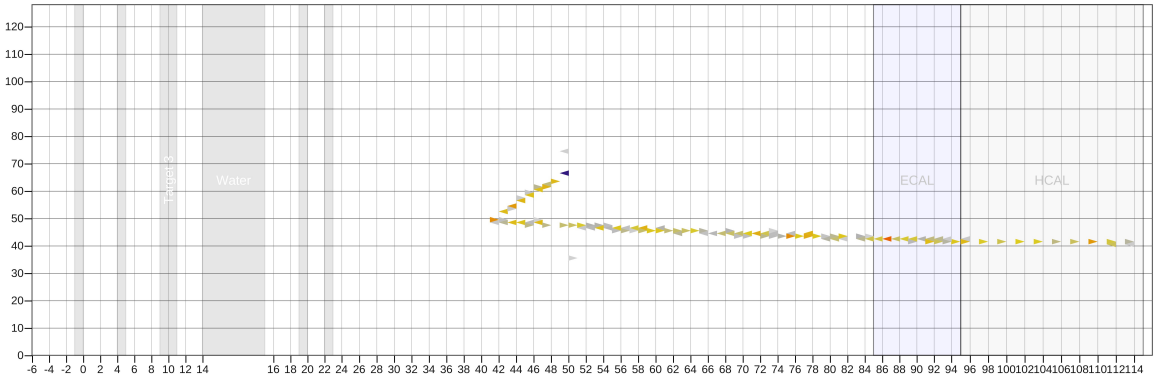

Figure 21: An increasing track

A track with debris or decay can have the same structure as either of the first two categories, but there is a trajectory change in the track or it contains small hits around the end of the track, signaling decay. Figure 22 contains a track with decay or debris. Pions may or may not do this, but low energy protons will rarely do this, preferring to simply run out of energy and stop.

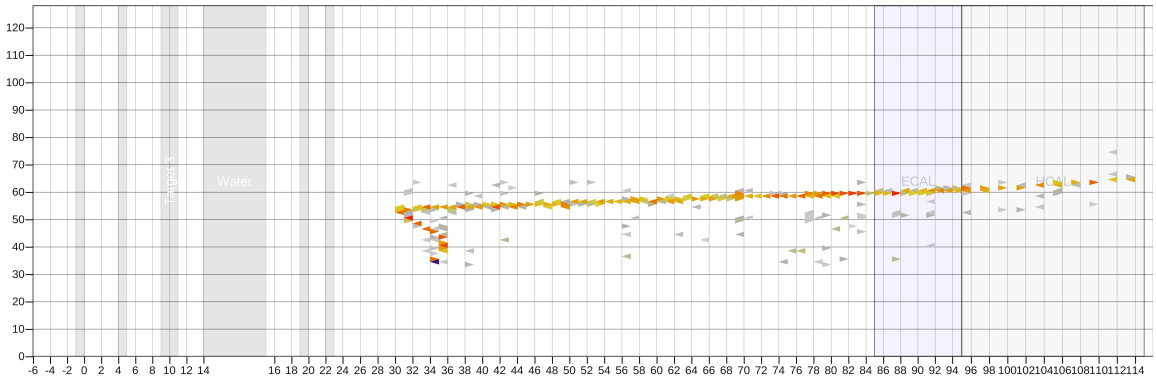

Figure 22: A track with debris or decay

The Michel positron category is also an attempt to identify pions. Pions will decay into a muon, which subsequently decay into positrons. Scanners checked at the vertex and at the end of tracks for these positrons later in time from the selected

event for evidence of pion decay. This category is in addition to the track categories, so regardless of classification of the event any Michel positron candidates were counted.

A set of 86 data events and 517 MC events were scanned by Alec Lovlein and Jake Leistico who are UMD undergraduates. The results are shown in table 10. The major discrepancies between the MC and data are seen in the uniform track category and the other category. Although the “other” category will be a mix of mostly protons and some pions, the uniform track category represents pions for which the MC has 11% more, which is equivalent to saying there are 40% too many pions in the MC.

	uniform track	heavy track	track with decay/debris	other	Michel positron
Percentage MC	37.1	14.9	13.9	34.0	53.0
Percentage Data	25.9	16.5	11.8	44.7	47.1

Table 10: The results from the delta scanning study

The MC needs less pions based on the delta scanning results. By decreasing the delta rate we would see improvement in this scan with MC events migrating from the uniform track category into the other and heavy track categories. These results showing too many pions matches the observation in the MINERvA result[17] and the Joint Theoretical and Experimental Seminar held 26th of June using the same data but a different selection methodology. This result will inform further model testing in the results section.

4 Initial Delta Systematics Study

Systematic uncertainty studies are a check to examine if changing parameters of the simulation would explain the data and MC discrepancies. The goal is to check that any inconsistencies in what we are already modeling in the MC simulation could not cause the discrepancies we are seeing in the recoil energy distribution. The first two groups of systematics which we investigated are the delta resonance creation in process by me, and resolution and biasing effects in our reconstructed quantities by Ethan Miltenberger.

There are multiple model components that make delta resonance production hard to model. Our examination of low q_3 for this analysis shows a deficit of the MC in the dip region as delta production is increasing and an excess of MC on the tail of the delta. Any error in calculating diagram level delta production, delta cross section measurements, and nuclear effects can make a huge difference in the model. Our goal is to determine if we can fix our delta agreement by making systematic changes to our delta model.

Delta production is identified by final state pions and reconstructed invariant mass. All types of delta baryons have a mean lifetime of 10^{-24} seconds. This produces a decay still contained inside the nucleus. If a pion escapes the nucleus, delta production can be identified by the appearance of a charged pion signature, or a neutral pion signature. If the pion does not escape the nucleus, delta events can also be identified by the invariant mass of the resulting particles in the detector. This identification method is limited by neutral pion or neutron creation. These particles may not deposit energy in the detector during the correct time slice, leaving lost energy that cannot be reconstructed. These effects make a correct delta model all the more important.

There are certain diagram level delta events that are not incorporated to our Genie simulation. Figure 23 shows one such scattering event. This two particle two hole (2p2h) reaction has delta kinematics, but a pion is never produced to propagate through the nucleus. The final state to propagate through the nucleus is two protons. It is uncertain what type of interference this diagram would have on delta production. It may be that these events must be added on top of the current Genie delta production model, or that for every event of this type one event from another delta diagram is removed. Either of these outcomes would produce less pions after final state interactions, or FSI.

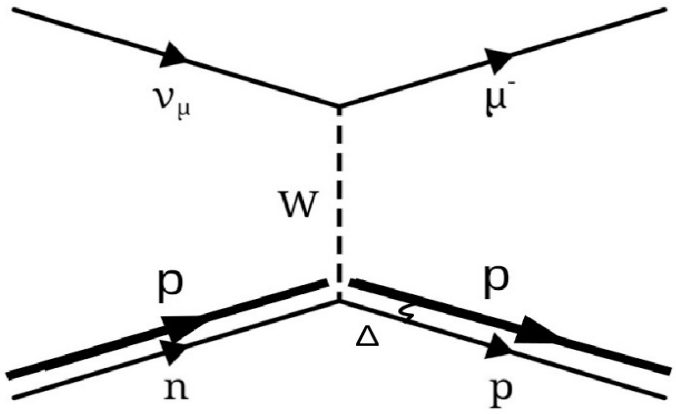

Figure 23: Feynman diagram for delta production with no pion produced, Nieves et all 2009

Nuclear effects are essential for modeling final state pion content for delta production. As the delta decays in the nucleus, the resultant proton and charged pion will re-scatter off of the other nuclei. Charged pions, consisting of a quark/anti-quark pair, have a high rate of interacting with other nuclei. These charged pions can be captured by the nucleus with another nucleon knocked out of the nucleus as a result. Improving modeling of FSI to produce the correct number of events without a charged pion in the final state could help in areas with an excess in the simulation.

By tuning FSI we can add or subtract final state charged pions. The default Genie comes with 75% of truth delta events with a pion in the final state, and 25% without a pion in the final state. We will attempt to discern if the model requires more or less pions.

Modeling delta production also requires an accurate cross section for such events. The measurements for the cross section of delta production was originally made on deuterium[14][15][16] with 20% uncertainties. This large uncertainty creates a real problem with the delta model. The goal of both MINERvA and MiniBooNE experiments is to make much more accurate measurements for these types of cross section calculations, around 5% uncertainty. These levels have not yet been achieved, so uncertainty in the delta cross section plays a role in our model deficiencies.

With all of these uncertainties in the various aspects of the delta production model it's not surprising there are multiple areas in the low q_3 section of our kinematic space in the region dominated by delta production. Through this initial delta systematic study and continuing into the error band analysis for delta systematics we will attempt different scales to delta production to attempt to improve

agreement between MC and data in these regions.

4.1 Testing the Dip Region

The delta region in low q3 overlaps with our dip region as QE events fall off and delta events increase. Since the dip region corresponds to an area where there is an under prediction of the standard genie model compared to the data, we would like to check if different delta prediction amounts could make up this discrepancy.

First, we tested to see if a boost of 20% more events with a pion in the final state. The standard distribution figure 25 is show below beside the distribution with a 20% boost of events with a pion in the final state in figure 24. The brown line in both plots is the total number of delta events. In figure 24 the red line shows the number of delta events with a pion in the final state, the quantity that has been boosted by 20%. The effect of this boost can be seen between 0.16 GeV and 0.26 GeV, as the ratio in figure 24 has improved in this delta region compared to figure 25. Although the ratio is closer to 1 at the high energy end of the dip region, it does not sufficiently make up the gap in the dip region. The ratio also becomes worse at the tail end of the high recoil energy section.

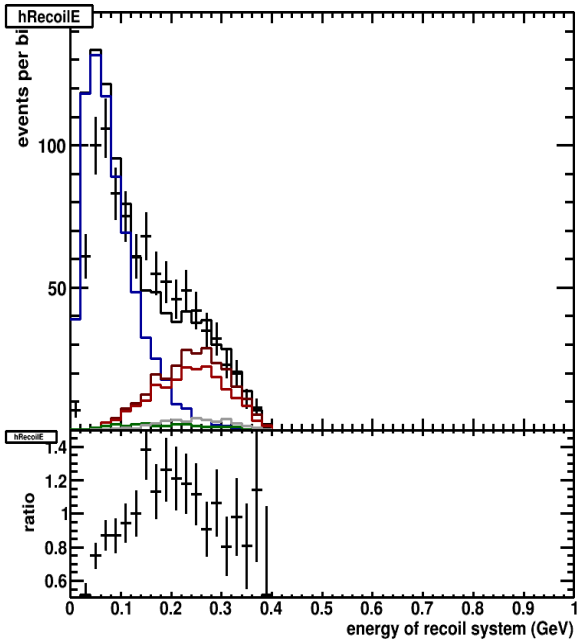

Figure 24: Low q_3 as a function of reconstructed recoil energy and delta with a final state pion events scaled 1.2. Data points are black dots. Total simulated events are solid black lines, while the blue and brown lines are the QE and delta subsets of the simulation respectively. The red line shows the delta events with a final state pion

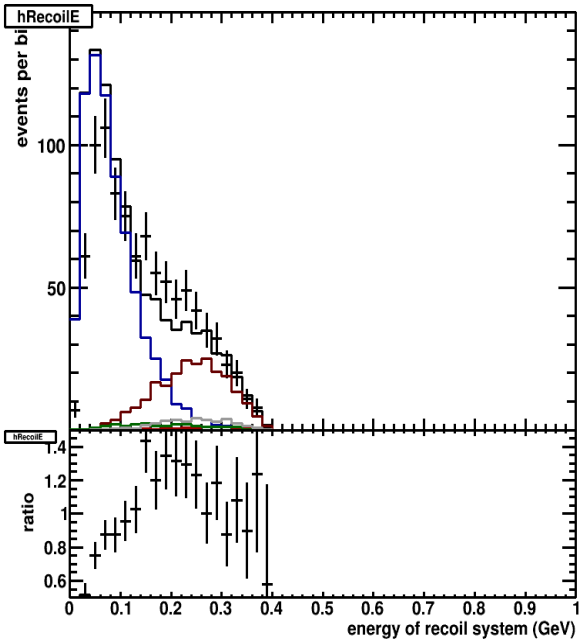

Figure 25: Standard Low q_3 as a function of reconstructed recoil energy Data points are black dots. Total simulated events are black lines, with the blue lines corresponding to the QE simulated events and the brown line are the delta simulated events.

We checked to see if our model for delta events without a pion in the final state was low, this a test to see if more FSI is required to lower the pion count. To identify a delta event a charged pion is the easiest indicator, followed by an invariant mass in the detector of the delta at 1.232 GeV. Data events may be more likely to have a neutron after FSI and thus have lower recoil energy than regular delta events.

We doubled delta production without a pion in the final state but kept the number of delta events constant with the original MC simulation. To achieve this all events without a pion in the final state were scaled by a factor of 2, while all events with

a pion in the final state were scaled by a factor of 0.669. The results are shown below with our standard distribution again in a repeat of Fig. 25, and the new delta model in figure 26. The brown line on both plots again is the total number of delta produced with the red line in figure 5 representing the number of events with a pion in the final state. The change produced is hardly noticeable because the recoil energy spectra is predicted to be only slightly different between the two components until the recoil energy is very low. A small effect can be seen starting with the 0.28 GeV bin and extending towards the recoil energy cut off.

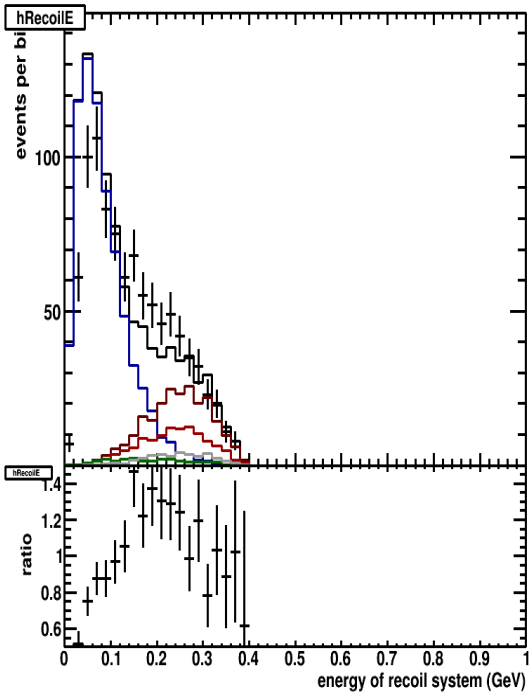

Figure 26: Low q_3 as a function of reconstructed recoil energy and delta with a final state no pion events scaled by 2. Data events are black dots, while total simulated events are black lines. The blue line shows QE simulated events, the brown line delta simulated events, the red line are delta with a final state pion

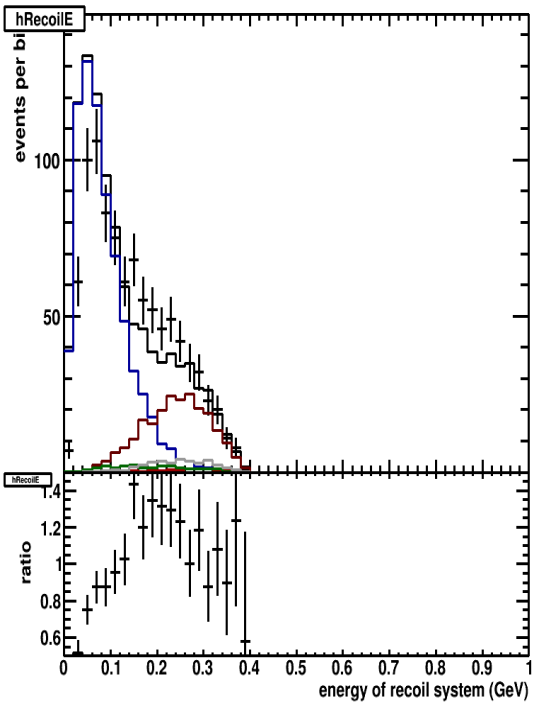

Figure 25:Standard Low q_3 as a function of reconstructed recoil energy Data points are black dots. Total simulated events are black lines, with the blue lines corresponding to the QE simulated events and the brown line are the delta simulated events.

Both of these tests for delta uncertainties show that our attempts to make up the MC deficit by altering delta production cannot make up these gaps. When boosting delta production with a pion in the final state by 20% we see that there are moderate gains made in the delta region, but does not flatten out the ratio in the dip region significantly. By doubling the events without a pion in the final state but keeping the total number of delta events constant, we cannot make up this deficit.

4.2 Particle Reconstruction Systematics

The MC simulation from Genie comes with truth information for each event it simulates, which is a very useful tool to investigate how accurate the reconstruction quantities are. We used this information to investigate how well our reconstructed recoil energy matched the truth energy of different particles. Our low q3 distribution is dominated by protons, which are products of both the neutrino QE process and also one of the decay products of delta production. There is also a healthy population of pions, also from the decay of the delta particle. We want to check how well the reconstructed recoil energy matches the truth energy of these particles.

To investigate, we plotted the truth proton energy against the recoil energy. Events were selected by requiring more than 5 MeV of truth proton energy, but less than 5 MeV of energy for all other types of particles. The distribution is shown in figure 27. The majority of events cluster and give us an idea of how accurately the protons were reconstructed. By eye we can see that there is a slope of close to 1.5 meaning that the reconstructed recoil energy is roughly 1.5 times higher on average than the truth information from that same event.

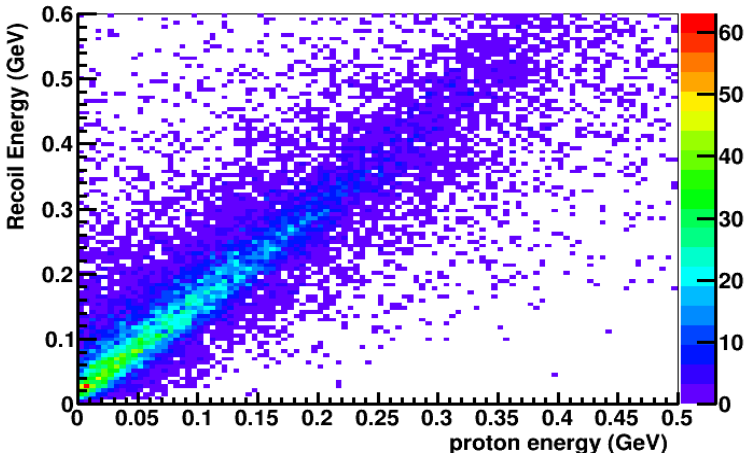

Figure 27: Intensity plot of event truth proton energy compared to the reconstructed recoil energy

Since the pion is the other dominant particle in our low q3 region, we can also model how the recoil energy responds to pions in the detector. Events were selected by requiring that the truth proton energy or truth pion energy be greater than 5 MeV, and the energy of all other particles is less than 5 MeV. The x-axis is the sum of the proton and pion energies, since we will now have events that are only proton, only pion, or protons and pions together. The common proton line can be seen immediately in the same spot in figure 28. The new events are now events with a pion involved, and these cluster in a different area.

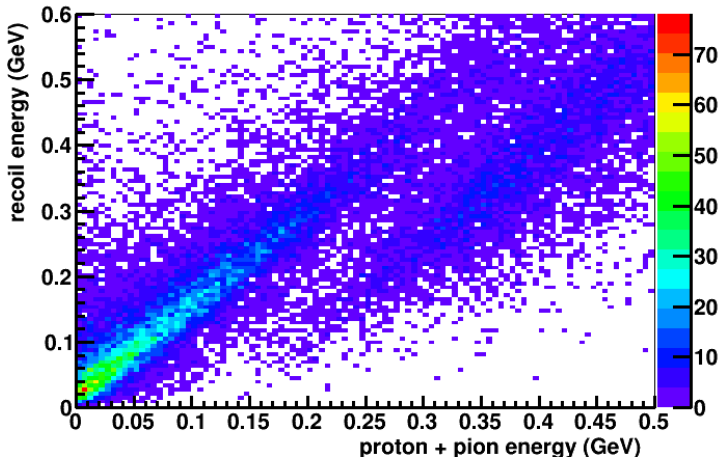

Figure 28: Intensity plot of event truth proton KE + pion total energy compared to the reconstructed recoil energy

The slope of the pion line is the same as the proton, but there is a shift in energy. The offset between the proton events and pion events is very close to the mass of the pion, or 0.139 GeV. This occurs because the truth total pion energy includes the mass of the pion. In other words, if the pion has zero kinetic energy the truth energy will be 0.139 GeV while the reconstructed recoil energy would be zero. The recoil energy, by design, is made to average these two reconstructed quantities. This offset was first noticed by Phil Rodrigues of the University of Rochester, and lead to the use of proton KE + pion total energy as a robust observable in our analysis.

5 Results

5.1 Unfolding

By a process called “unfolding” the data allows model additions such as RPA and MEC to be added to Genie for comparison to the default simulation. Unfolding is the process of using the truth event information for the MC and comparing where these events are reconstructed. Even if the number of events in a particular true data bin is unknown, the MC knows what fraction of those events will end up in each reconstructed bin. We can analyze this migration and apply it to the reconstructed data to achieve truth like data. With unfolded truth like data any truth Genie model can be compared. Models more complex than a reweighing of fully simulated events (such as our RPA model) cannot be tested against our reconstructed values because new models have not been run through GEANT 4 for detector simulation.

Unfolding requires a migration matrix to track how q_0 is reconstructed compared to the truth q_0 values. Reconstructed MC energy visible in the detector is compared to true available energy from the Genie truth quantities. Figure 29 shows the migration matrix for our low energy, low q_3 sample. For the reconstructed visible energy variable we used passive corrected energy in the tracker + ecal x 1.12. The factor of 1.12 is used to produce an unbiased energy estimate, but does not affect the unfolding procedure. Truth available energy is truth values for proton KE + pion KE + pizero E + gamma E + electron E.

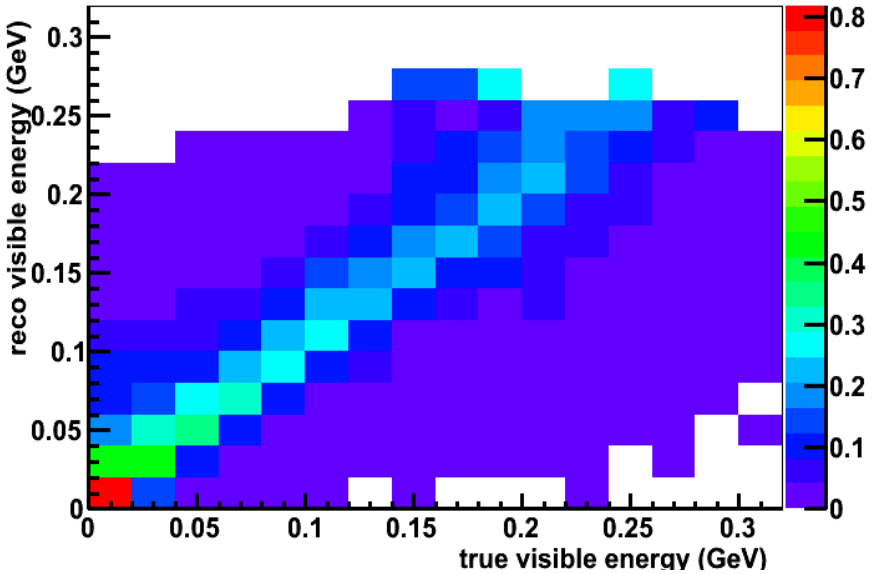

Figure 29: The migration matrix for this analysis

For each reconstructed energy bin, the migration matrix tracks the percentage of events events that had truth energy values. Moving in a horizontal row, each color represents the fraction of events, and will add up to 1 with all bins summed.

The inverted migration matrix is used to create truth like data. Data events are taken from each reconstructed energy data bin, and are placed in truth like energy data bins. With this truth like data any model, including our Genie model with the RPA and MEC models added, can be placed next to the data for comparison without a full detector simulation.

An acceptance correction histogram is also necessary to account for a different migration of events in and out of our low q_3 sample. To account for this, we take a ratio of the truth q_3 to the reconstructed q_3 for each event. A scaling factor is created for each bin which is then applied after the unfolding process. Figure 30 shows the acceptance correction histogram for our low q_3 sample. At a truth

available energy less than 0.12 GeV after unfolding the truth like data is multiplied by a scaling factor greater than 1. Events in this region need to be scaled up after unfolding to account for a migration of events that is preferentially out of the low q_3 sample into the mid q_3 sample. Greater than 0.12 GeV produces a scaling factor of less than 1 or a reduction of events in these bins. These migration effects were studied by Ethan Miltenberger in his thesis.

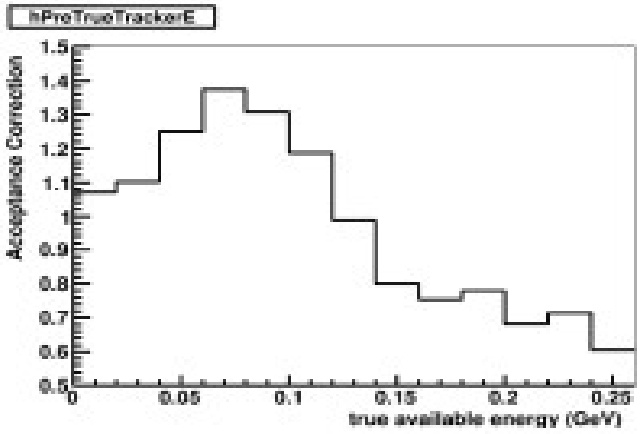

Figure 30: Acceptance correction for unfolding in our analysis

5.2 Unfolding Results

With the unfolding technology in place, we are able to compare our original low q_3 distribution to the unfolded distribution. Figure 31 is the original low q_3 distribution using reconstructed energy in the tracker + Ecal as the x-axis, while figure 32 is the unfolded distribution with the unfolded available tracker energy on the x-axis. Figure 32 was made by applying the migration matrix in figure 29 and then using the acceptance correction in figure 30 to unfold the data, which is compared to MC truth available energy. In both figure 31 and figure 32 data is

represented by the black points, while the MC is shown with a black solid line with QE components in blue and delta components in red. In figure 31 the data error bars are statistical uncertainties of size √n. The same is true for figure 32, although with this unfolding process we know we have overestimated the unfolded statistical uncertainty. The statistical uncertainty on the unfolded data is too large because the correlation of the uncertainty between bins due to unfolding has not been factored in to our procedure yet.

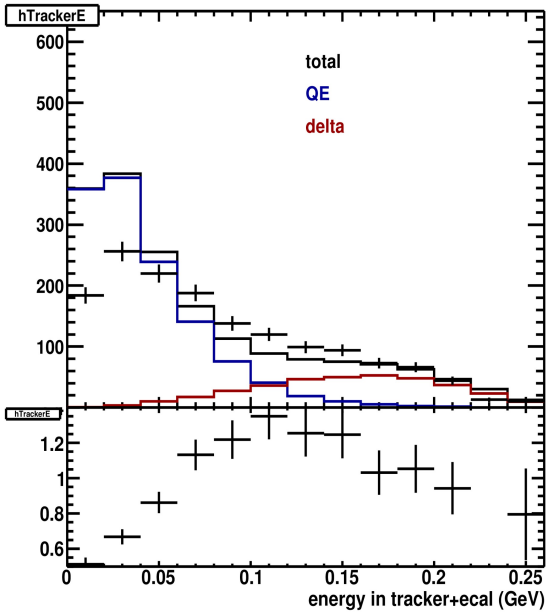

Figure 31: Reconstructed low q_3 histogram using energy in the tracker + ecal

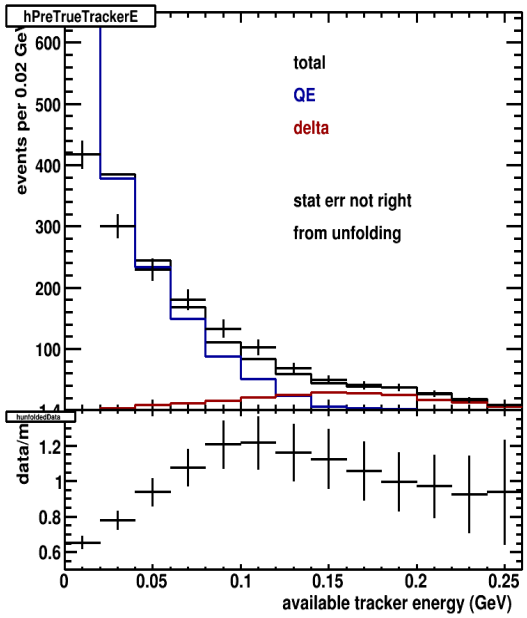

Figure 32: Unfolded low q_3 histogram using the migration matrix in figure 1 and the acceptance correction in figure 2. Data statistical error bands are too large

5.3 Error Bands

In order to compare the results with and without RPA and MEC models, we need an error band based on our systematic uncertainties studies. In the previous chapter we explored if uncertainties in the MC delta models could make up the

discrepancy between reconstructed MC and data. Although our results show these delta model uncertainties do not make up this discrepancy, these uncertainties can be combined in quadrature together to produce and error bar. Using the results of the delta uncertainties we can draw an error bar on the MC for our reconstructed quantities.

Using the unfolding process these uncertainties propagate into the unfolded data producing an error bar on the unfolded data. This error bar will be combined with the statistical uncertainty from the unfolded data. We can compare these delta uncertainty error bands with Ethan Miltenberger's results from detector resolution and biasing effects.

To determine the delta systematic error bars we boost delta production 20%, reduce delta production 20%, and double the delta with a final state without a pion while keeping the overall delta production constant. These tests mirror the worst case scenarios for errors in the Genie delta production model. The reconstructed delta systematics results are shown in figure 33, while the propagated unfolded results are shown in figure 34.

Boosts and reductions of 20% behave as expected. In both Fig. 33 and Fig. 34 the red line corresponds to a delta boost of 20% while the green corresponds to a delta production reduction of 20%. To produce the ratio plots below, each of these systematic instances is divided by the default MC, which is represented by the black data points with error bars. For boost delta production 20%, the red line shows the ratio increase to greater than one starting at 0.06 GeV, corresponding to the region in which we start to see delta production. Conversely the reduction of delta 20% has the opposite effect.

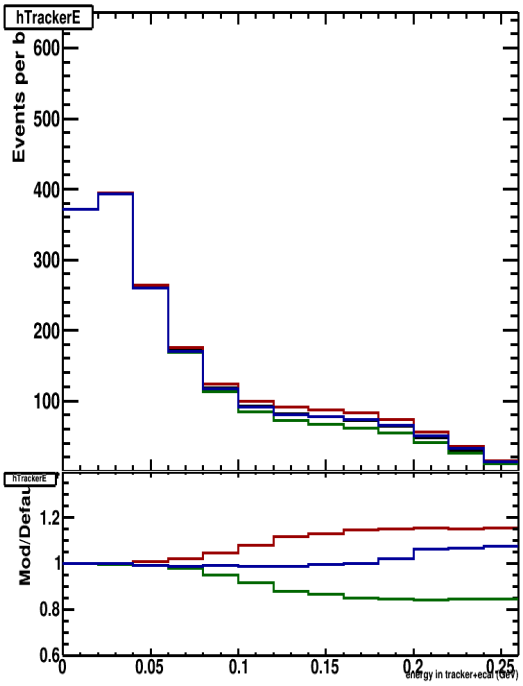

Figure 33: The reconstructed results for 20% boost in delta production (red line,) a 20% reduction in deltas (green line,) and a 50% boost in the delta with no pion (blue line)

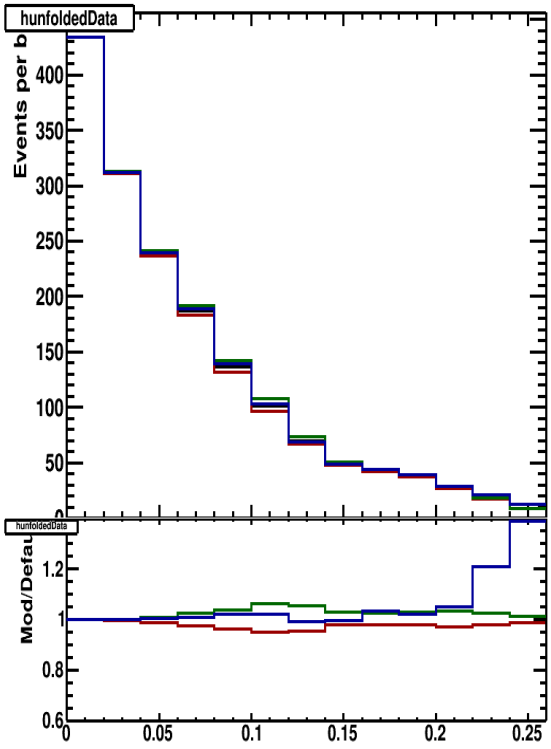

Figure 34: The unfolded results for 20% boost in delta (red,) a 20% reduction in delta (green,) and 50% boost in the delta with no pion (green)

Figure 34 shows the results of unfolding these effects. By construction the errors are symmetric around 1 and remain so after unfolding. These effects never reach a full 20% because the QE process still has a non-zero event rate throughout low q_3. By unfolding the different delta systematics we are changing the migration and acceptance rather than the model itself.

In figures 33 and 34 the blue line corresponds to delta without pions boosted 50% while the overall rate of delta kept constant. The figure 33 ratio plot shows that this results in a mostly flat ratio of one, with a 5 to 10% effect towards the end of

the distribution, starting at 0.18 GeV. This corroborates the results from the earlier systematics study that delta without pion in the final state is fairly equally distributed within the delta.

Unfolding produces similar results, with one exception. Figure 34 shows a ratio around one for this effect until 0.22 GeV, where the ratio increases greatly. Normally the unfolding process has a smaller effect because the rate of the uncertain process does matter as much, only how it migrates differently around the sample, so this result was surprising. The large effect is due to a changed acceptance correction for the deltas without pions boosted 50%. Figure 35 illustrates how different the acceptance correction for this systematic uncertainty study. The final two bins differ greatly between Fig. 35 and Fig. 30, which is the acceptance correction for our analysis with no systematic uncertainty study. This result shows that delta's with a pion will preferentially migrate into our low q_3 sample from mid q_3 after unfolding, but delta's without a pion will not. Enhancing the latter gives less migration overall.

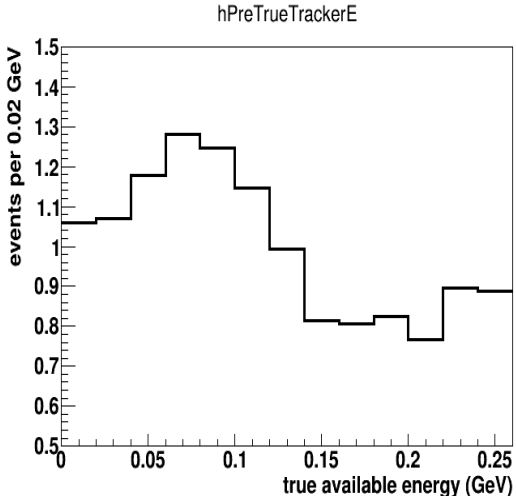

Figure 35: Acceptance correction when pionless deltas are boosted 50% but the overall delta rate constant

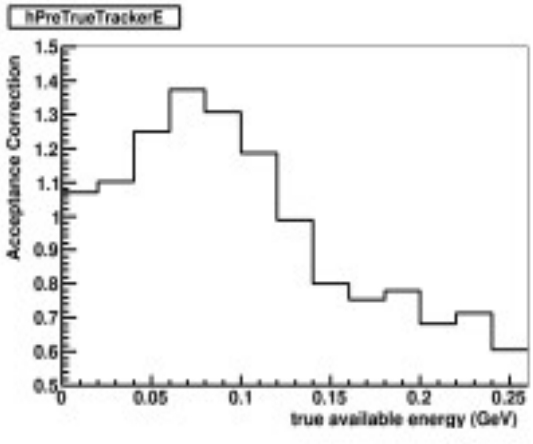

Figure 30: Acceptance correction for unfolding in our analysis, repeated for comparison

Migration to and from the mid q_3 sample is not affected by whether the final state has neutrons or not. The ratio of truth proton energy to truth proton and neutron energy is shown in figure 36. The Genie model has 123 events with proton only final states, seen at the value of 1 on the right side of the figure. There are 911 events with final states having neutrons, with less than 25 neutron-neutron final states as is expected from neutrino charged current scattering. For proton-neutron final states the sharing of this energy is peaked at 50%. Delta's without pion are composed of protons and neutrons, so we examined the proton and neutron energy sharing for these pionless delta events.

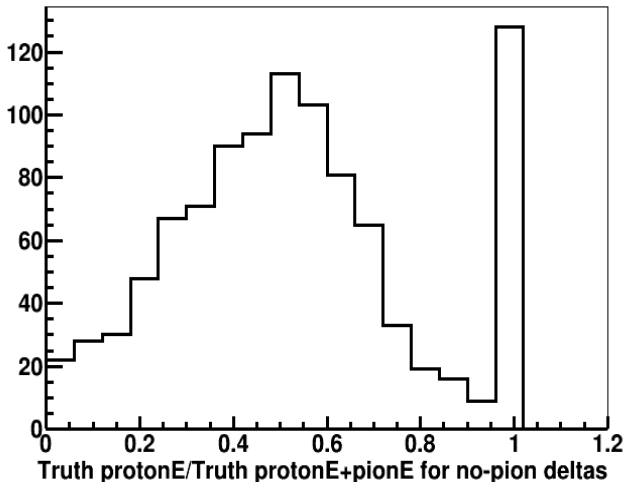

Figure 36: The ratio of truth proton energy to truth proton plus neutron energy for pionless deltas.

Most events in Fig. 36 have protons and neutrons in the final state. Proton-only final states have higher resolution than neutrons and their recoil energy is biased higher than the truth proton energy as seen in figure 27. Having some neutrons in the final sate yields worse resolution and in the extreme might have their recoil energy biased near zero. At this time we have not concluded (independently of Fig. 35 like Fig. 27) that the mix of proton+neutron final states are also biased high

relative to pions, and thus cannot determine if the migration effect is because of biasing effects in the recoil energy or because of the worse resolution inherent with neutrons.

An important prediction from this study follows because the GENIE final states from the pionless deltas is opposite what is predicted in Nieves model for deltas. GENIE has 88% with neutrons in the final state, while Nieves predicts 75% proton-proton final states as shown in figure 37,[3] and closer to 80% in the delta region. In the figure, these are shown as coming by way proton+neutron initial states where the neutron becomes a proton in the charged-current reaction. These not yet simulated proton+proton Nieves' MEC events are predicted to have even higher resolution and less migration than these pionless delta GENIE events.

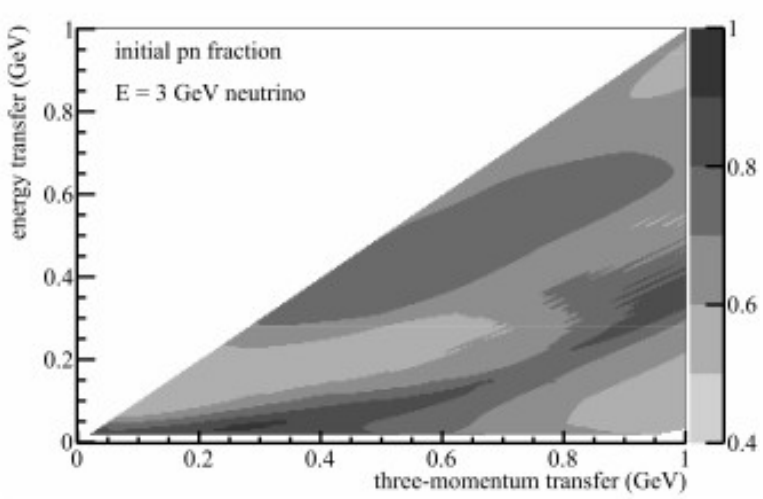

Figure 37: Initial proton-neutron faction for the Nieves model from the 2013 PRD calculation [3]

These three errors are combined for a delta error bar. The effect of each of these shifted delta scenarios for the reconstructed quantities can be found in table 11. The first two columns correspond to the energy values bookending the bin in GeV.

Column three represents the default GENIE MC with no delta scaling. Columns four and five correspond to the red and blue line from figure 5 respectively. These numbers express the difference between the default GENIE, and the resultant delta uncertainty GENIE. The final column is the quadrature summed values from column four and five as if they were symmetric effects. As we see from Fig. 33 there is little to no change to the bins below 0.04 GeV of q_0. The largest effects are seen at the peak of the delta, between 0.12 and 0.22.

Low Bin (GeV)	High Bin (GeV)	Default Genie	Boost 20%	No Pion Boost	$\sum_i(\Delta_i^2)$
0	0.02	359.31	0.08	0.08	0.11
0.02	0.04	383.44	0.67	-0.17	0.70
0.04	0.06	255.29	1.99	-1.32	2.39
0.06	0.08	166.11	3.44	-2.14	4.05
0.08	0.1	113.29	5.48	-1.36	5.65
0.1	0.12	88.82	7.17	-1.42	7.31
0.12	0.14	78.89	9.28	-0.97	9.33
0.14	0.16	75.36	10.02	-0.28	10.02
0.16	0.18	70.76	10.56	-0.10	10.56
0.18	0.2	62.69	9.61	1.51	9.73
0.2	0.22	46.68	7.37	3.07	7.98
0.22	0.24	30.21	4.59	2.27	5.13
0.24	0.26	12.58	1.91	0.54	1.99

Table 11: Calculation of the error based on the difference between the standard Genie model and each systematic explored for the reconstructed quantities

The same method can applied to the unfolded data from figure 34. The results are in table 12. After unfolding, the boosting and reducing delta 20% figures are nearly symmetric as before, although now unfolding has smeared these events asymmetrically. The quadrature summed uncertainty numbers are smaller in general, although we can see in the highest energy bins the no pion boost returns very high uncertainty compared to the number of events in the default GENIE. For example a 3.27 uncertainty in the highest bin, from 0.24 to 0.26 GeV, gives a ratio to the default GENIE of 1.39, which corresponds to the final bin ratio in figure 34.

Low Bin (GeV)	High Bin (GeV)	Default Genie	Boost 20%	No Pion Boost	$\Sigma_i(\Delta_i^2)$
0	0.02	417.18	-0.09	0.13	0.16
0.02	0.04	300.27	-0.58	0.33	0.67
0.04	0.06	229.39	-2.28	0.97	2.48
0.06	0.08	180.38	-4.19	1.70	4.52
0.08	0.1	133.20	-4.62	2.42	5.22
0.1	0.12	102.31	-5.21	1.94	5.56
0.12	0.14	68.42	-2.95	-0.31	2.97
0.14	0.16	49.10	-1.00	-0.46	1.10
0.16	0.18	41.05	-0.73	1.32	1.51
0.18	0.2	37.29	-0.71	1.00	1.23
0.2	0.22	26.47	-0.65	1.22	1.38
0.22	0.24	16.85	-0.30	3.48	3.50
0.24	0.26	8.30	-0.09	3.26	3.26

Table 12: Calculation of the error from the difference between the standard Genie model and each systematic explored for unfolded quantities

The total uncertainties column can be used to create our error bars. The values from table 11 are used to draw error bars on the subsequent reconstructed MC plots. Table 12 is used to draw error bars on the subsequent unfolded data plots. With these delta uncertainty error bars we can now compare the delta systematic uncertainties to Ethan Miltenberger's detector resolution results as well as add the RPA and MEC models to GENIE.

5.4 Detector Resolution and Biasing Uncertainties

Parallel to the delta systematic uncertainties study shown here, Ethan Miltenberger produced uncertainty and error bars for detector resolution and biasing effects. They are summarized here so we can use them to interpret the model agreement with the data.

Resolution and biasing effects deal with how the detector takes a real event and

reconstructs the different energy values we use to analyze the events. Biasing effects smear quantities one way or another uniformly for all events commonly through uncertainties in calibrations and energy scales. These effects will move events around our distributions, and depending on energy cuts made during our analysis, could migrate certain events in and out of our sample. Both q_0 and q_3 are reconstructed quantities and are effected by resolution and biasing.

Resolution and biasing effects were studied by varying the recoil energy q_0, muon energy, and muon angle by their known quantities. The nominal resolutions were determined by taking the reconstructed MC value of our variable and taking the ratio with the truth MC for our specific low q_3 sample. The resolution quantities used are 50% for q_0, 8% for muon energy, and 10 mrad for the muon angle.

Uncertainties that bias reconstructed quantities have been determined by the MINERvA collaboration for their detector. The standard biasing value is 2.6% for the muon energy and 1 mrad for the muon angle. A biasing value of 5% for hadron energy scale accounts for several different effects including the updated test beam result, but is not the standard reported MINERvA bias.

Resolution values were also degraded in case our resolution is worse than reported by the study between reconstructed and truth q_0. The value of q_0 was degraded to a 55% resolution while the muon energy was degraded to an 11% resolution.

Results for the degraded resolution and biasing error bars for the reconstructed data are show in table 13, and are taken from Ethan's Thesis. Column three is the total uncertainty due to all biasing effects tested while column four is the uncertainty due to degraded resolution effects. All of the biasing and resolution effects are summed for the total error band, which is column five.

Bin Low	Bin High	$\sum_i(\Delta^2_{bias})$	$\sum_i(\Delta^2_{res})$	$\sum_i(\Delta^2_{tot})$
0.0	0.2	8.80	7.46	11.54
0.2	0.4	13.11	11.01	17.12
0.4	0.6	13.38	9.09	16.18
0.6	0.8	11.25	7.86	13.72
0.8	1.0	8.75	4.42	9.80
1.0	1.2	7.56	5.33	9.25
1.2	1.4	5.15	1.65	5.41
1.4	1.6	5.38	3.67	6.51
1.6	1.8	5.48	3.23	6.36
1.8	2.0	7.93	2.94	8.46
2.0	2.2	9.50	1.55	9.62
2.2	2.4	10.11	6.56	12.05
2.4	2.6	7.72	15.52	17.33

Table 13: Error bar results from Ethan Miltenberger's resolution and biasing studies for reconstructed values

Bin Low	Bin High	$\sum_i(\Delta^2_{bias})$	$\sum_i(\Delta^2_{res})$	$\sum_i(\Delta^2_{tot})$
0.0	0.2	15.64	9.94	18.53
0.2	0.4	14.52	8.98	17.08
0.4	0.6	13.21	8.19	15.54
0.6	0.8	12.24	6.77	13.99
0.8	1.0	10.75	5.90	12.26
1.0	1.2	8.29	3.74	9.09
1.2	1.4	6.36	2.57	6.86
1.4	1.6	5.56	1.80	5.85
1.6	1.8	5.23	1.29	5.39
1.8	2.0	6.27	3.39	7.13
2.0	2.2	6.39	3.70	7.39
2.2	2.4	3.90	4.44	5.91
2.4	2.6	2.54	3.36	4.21

Table 14: Error bar results from Ethan Miltenberger's resolution and biasing studies for the unfolded values

Biasing and resolution effects are significantly greater in the lowest energy and highest energy bins, and delta effects are greater in the dip region, except for the delta test where we increased the no pion content. We can compare the total delta error bars found in table 11 to Ethan's figures for resolution and biasing error bars in table 13. The total error bar from 0.0 GeV to 0.1 GeV is significantly higher for Ethan's in the lowest bins, with the effects nearly equal at 0.1 GeV. From 0.12 GeV to 0.2 GeV the uncertainty for delta is higher than the resolution and biasing uncertainty, although the resolution and biasing effects are significant with values ranging from 5.41 to 9.80. At the end of the distribution the delta uncertainty decreases and there is a major spike in uncertainty in the last bin.

After unfolding uncertainty is dominated by the resolution and biasing effects. The unfolded delta uncertainty in table 12 is flattened out by the unfolding process. There is no longer a peak of uncertainty values corresponding to the delta peak, it has been replaced by a much less sharp peak from 0.04 to 0.14 GeV. Compared to

the delta uncertainty, the resolution and biasing uncertainties are higher for every bin in table 14. To compare default Genie to a Genie with RPA and MEC added we will use the unfolded distribution for which the uncertainty is dominated by resolution and biasing effects.

5.5 RPA and MEC Model Results

RPA and MEC model additions are predicted to improve the discrepancy between MINERvA's data and MC distributions. Figure 38 shows the reconstructed distribution with statistical and delta systematic uncertainties. This plot is equivalent to figure 31. For reconstructed values we can add in the RPA effect since it is a scaling and is not dependent on the GEANT4 detector simulation. The proposed RPA model scales down events in the QE range exactly where we see an overabundance of MC events. The scale is applied to each fully simulated event by applying a weight as a function of q_0 and q_3 derived from Juan Nieves' calculation. The reconstructed distribution with the RPA effect added is figure 39. The ratio below these plots is the ratio of data/MC, for which the RPA effect in Fig. 39 flattens the ratio in the low end of the distribution, up to 0.04 GeV.

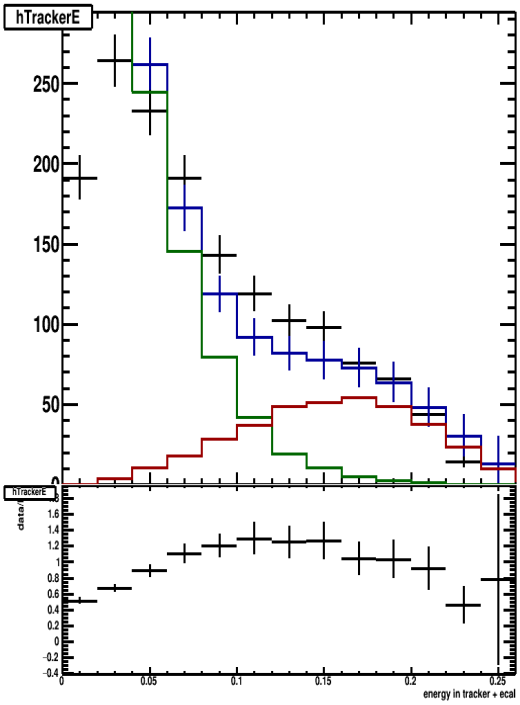

Figure 38: Standard reconstructed low q3 distribution with energy in the tracker + ecal. QE and delta components of the blue simulation are shown in green and red

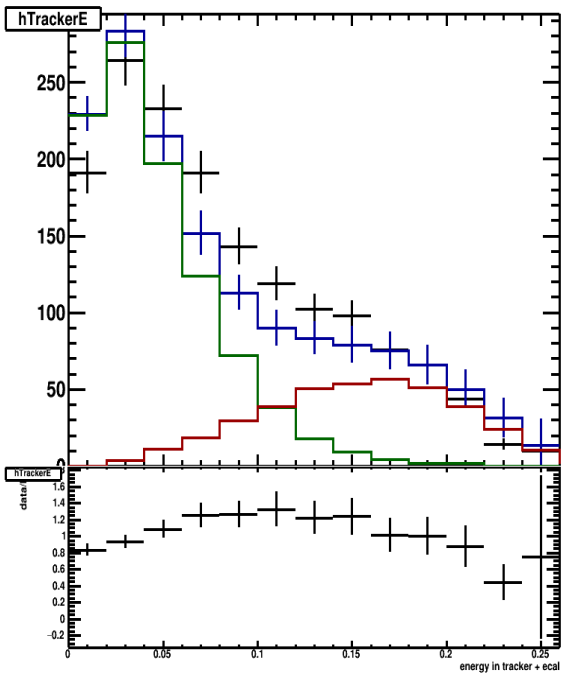

Figure 39: Reconstructed low q3 with RPA effect added with energy in the tracker + ecal. QE and delta components of the blue simulation are shown in green and red

After unfolding we can test any models we so choose. The MEC model cannot be added to the reconstructed distribution because of GEANT4 detector effects, but can be added with the RPA to the unfolded distribution. Figure 40 shows the unfolded distribution with no additional model effects. This is equivalent to figure 32. Figure 41 shows the results from adding just the RPA model. As in the comparison to between Fig. 38 and 39, adding the RPA effect to the unfolded distribution greatly flattens the ratio between the lowest bins in the distribution. It continues to have no effect as energy increases.

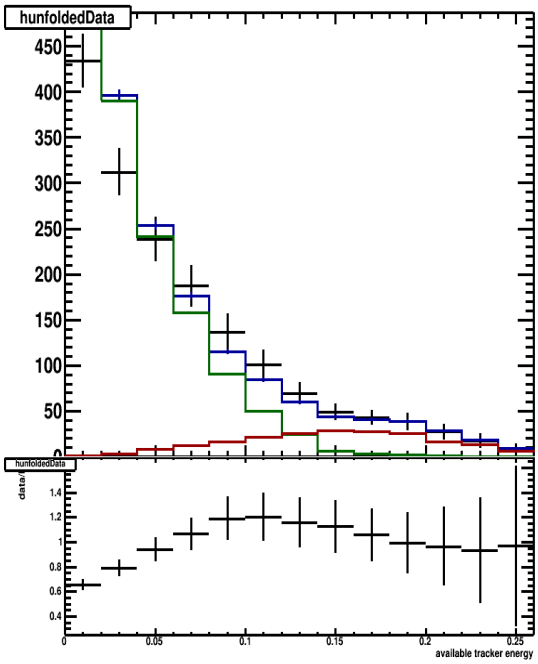

Figure 40: Standard unfolded low q3 distribution with available tracker energy. QE and delta components of the blue simulation are shown in green and red.

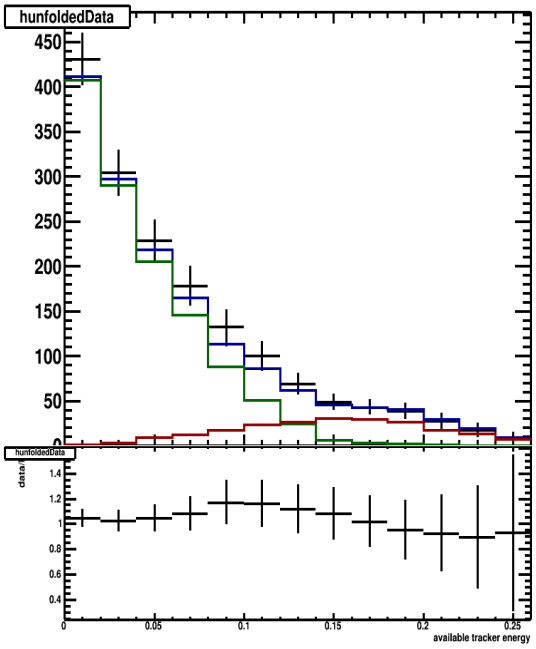

Figure 41: Unfolded low q3 distribution with the RPA effect added with available tracker energy. QE and delta components of the blue simulation are shown in green and red.

Adding the MEC model continues to help flatten out the ratio in the dip region. Figure 42 shows the unfolded distribution with both the RPA and MEC effects added. As the MEC effect is added the ratio increases in the lowest available tracker energy bins due to normalization effects, but the ratio from the zero bin through the dip region is flat with very little fluctuation. The MEC model increases the size of the discrepancy in the delta peak region of the distribution, but we believe further delta model tuning could flatten this ratio out.

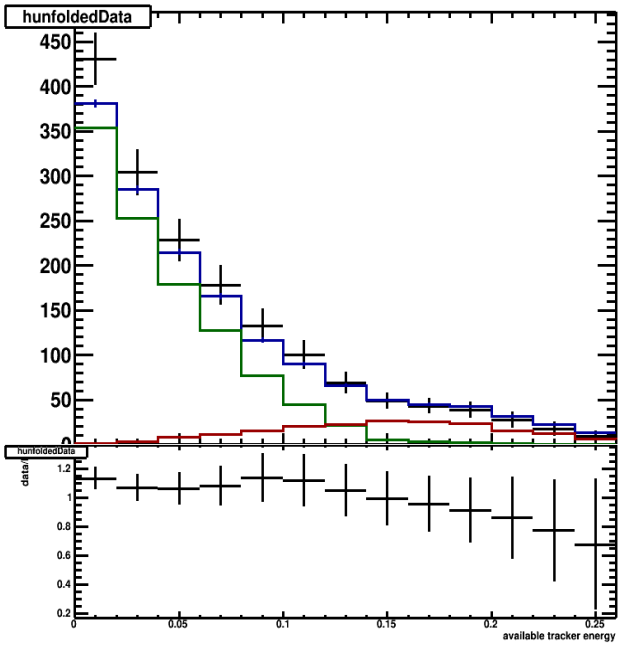

Figure 42: Unfolded low q3 distribution with the RPA and MEC models included with available tracker energy. QE and delta components of the blue simulation are shown in green and red.

Adding a 20% reduction of the total delta production with the RPA and MEC models continues to improve the ratio in the last few bins of our low q_3 sample. Adding this extra model addition was inspired by the delta scanning study in section 3.11. The results are shown in figure 43. The ratio in the dip region is increased slightly by reducing delta production in this area (so less flat). On the other hand, the right side of the distribution moves 15% closer to flat, similar to Fig. 33, improving overall agreement. Even with three changes to the model, the agreement is not perfect. However with modification to the model, and including all the other systematics show in the error bars, the model seems adequate to describe the data.

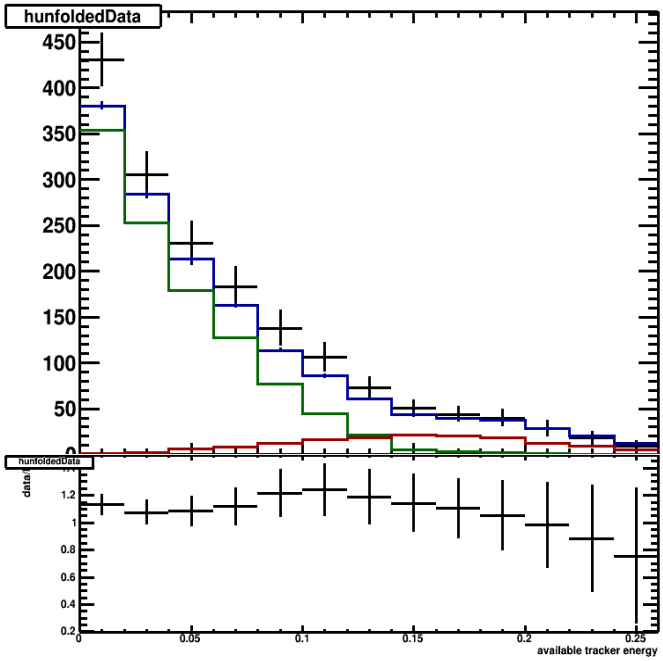

Figure 43: Unfolded distribution with the RPA and MEC models added and delta production reduced 20%. QE and delta components of the blue simulation are shown in green and red.

5.6 Model χ^2 Calculation

A χ^2 calculation can be made to quantify the improvement made by each model addition to our unfolded distributions. χ^2 is defined as

$$\chi^2 = \Sigma_i[(D_i - MC_i)^2/ \sigma_i^2] \qquad (14)$$

where D_i is the number of data events in each bin, MC_i is the number of MC events in each bin, and σ_i is the uncertainty for that bin. This calculation gives us a quantitative result on how each model added between Fig. 40-43 improve the

discrepancy between the simulated events and detector data events.

The results of the χ^2 calculation are show in Table 15. The statistical errors used in our unfolded error bar study are too large and doesn't respect the correlation between bins after the unfolding process. This issue is to be addressed with better software as our analysis continues. The systematic errors are correlated, but we are not using only these to draw the error bar. For this reason, the χ^2 will be unnaturally low and the $\Delta\chi^2 = 1$ probably does not apply. These results are shown in the first column of Table 15.

Model	χ^2	Best Normalization χ^2	Normalization Scale
Standard Genie Unfolded	73.72	34.4	0.81
Genie + RPA	3.47	1.68	1.05
Genie + RPA + MEC	6.67	4.0	1.07
Genie + RPA + MEC - Delta	9.86	2.35	1.11

Table 15: Results from the χ^2 study for Figures 40-43. The first column shows the normalization dependent χ^2 calculation, while the second column shows the shape dependent χ^2 with the MC normalization used listed in column 3

To calculate a shape dependent χ^2, a scale was applied to the MC results. Each model has a different normalization but by finding a minimum value for χ^2 we check for a shape dependent χ^2 which negates these normalization effects. Table 15 shows that for both methods, a standard Genie model with the RPA effect added has the best fit of all the unfolded models. Also of note is that the calculated χ^2 gets worse, and then better as the MEC and reduced delta models are added respectively.

6 Conclusions and Discussion

The RPA and MEC model additions improve the agreement between the data and MC. The RPA effect shows improvement between the data and MC in the QE region in both the reconstructed and unfolded distributions. The MEC model is only available for comparison to the unfolded distribution, but further improves agreement in the dip region.

Eye scanning of events was done in an effort to identify MEC model candidates with two proton final states. The results yielded a discrepancy between the data and MC between the 0 hadron and 2+ hadron categories. We attempted to distinguish between different types of final state events in the dip region where the MEC model predicts a cross section enhancement by using the MC truth. Two approaches, counting 10 MeV hits and 10 MeV hits in the vertex region were attempted. Both approaches could not distinguish between 1 proton truth events and 2 proton truth events, although they could distinguish proton events from pion and neutron events.

Scanning events were also weighted using the RPA effect, which improved the discrepancies between the scanned data and MC events but did not fully reconcile the discrepancies. Reducing the rate of delta resonance interactions would shift events from the 2+ hits categories further improving this discrepancies.

Delta systematic uncertainties were addressed as a means to improve the data and MC discrepancies, on top of the addition of the RPA and MEC models. Without the latter, the delta systematic uncertainties do not account for this discrepancy. The uncertainties from Ethan Miltenberger's detector resolution and biasing were larger than the delta uncertainties and also did not make up the discrepancies.

When the RPA and MEC models were added, the data is described by an MC at the edge of its systematic uncertainty.

An additional scanning study was done in the delta region. This study showed the MC had an excess of pions and informed further model additions by decreasing delta production by 20%. Addition of this continues to improve the discrepancies between data and MC when added with the RPA and MEC models.

Citations

[1] L. Fields et al. Measurement of muon neutrino quasielastic scattering on a hydro-carbon target at e ν ≈ 3.5gev. Phys. Rev. Lett., 111:022502, Jul 2013.

[2] Juan Nieves. Approximate methods for nuclei (ii) - part 1 of 3. Presentation at NuSTEC, October 26, 2014.

[3] F. Sanchez R. Gran, J. Nieves and M. J. Vicente Vacas. Neutrino-nucleus quasi-elastic and 2p2h interactions up to 10 gev. arXiv.org, arXiv:1307.8105 [hep-ph].

[4] J. Nieves, J. E. Amaro, and M. Valverde. Inclusive quasielastic charged-current neutrino-nucleus reactions. Phys. Rev. C, 70:055503, Nov 2004.

[5] David Pines and David Bohm. A Collective Description of Electron Interactions: II. Collective vs Individual Particle Aspects of the Interactions. Phys. Rev. 85, 338, 15 January 1952

[6] Arachne - A web-based event viewer for MINERvA N. Tagg et al. [MINERvA Collaboration]. arXiv:1111.5315 [hep-ex] Nucl. Instrum. Meth. 676, 44 (2012).

[7] Carrie McGivern. The story of a detector, and its daq. Presentation at MINERvA 101, slide number 3, June 16, 2014.

[8] Design, calibration, and performance of the MINERvA detector. arXiv.org,

arXiv:1305.5199 [physics.ins-det].

[9] MINERvA neutrino detector response measured with test beam data – arXiv:1501.06431.

[10] R. L. Kustom, D. E. Lundquist, T. B. Novey, A. Yokosawa, and Frank Chilton. Quasielastic Neutrino Scattering. Phys. Rev. Lett. 22, 1014, 12 May 1969

[11] W. A. Mann et al. Study of the Reaction $\nu+n \rightarrow \mu^{-}+p$. Phys. Rev. Lett. 31, 844, 24 September 1973

[12] C. Andreopoulos et al., The GENIE Neutrino Monte Carlo Generator, Nucl.Instrum.Meth.A614:87-104, 2010.

[13] S. Agostinelli et al., Geant4—a simulation toolkit, Nucl.Instrum.Meth.A 506:250-303, 2003.

[14] S. J. Barish et al., Study of neutrino interactions in hydrogen and deuterium. II. Inelastic charged-current reactions, Phys. Rev. D 19, 2521, 1 May 1979

[15] G. M. Radecky et al., Study of single-pion production by weak charged currents in low-energy νd interactions, Phys. Rev. D 25, 1161, 1 March 1982

[16] Callum Wilkinson, Philip Rodrigues, Susan Cartwright, Lee Thompson, and Kevin McFarland, Reanalysis of bubble chamber measurements of muon-neutrino induced single pion production, Phys. Rev. D 90, 112017, 24 December 2014

[17] B. Eberly et al., Charged Pion Production in νμ Interactions on Hydrocarbon

at ⟨Eν⟩= 4.0 GeV, arXiv.org, arXiv:1406.6415 hep-ex